https://doi.org/10.5194/egusphere-2026-4287
Preprint. Discussion started: 17 August 2026

Assessing trends in irrigation water withdrawal using a data-driven temporal extrapolation framework

Paul Zarpas[1], Maria-Helena Ramos[1], Gaëlle Tallec[1], Denis Allard[2], and Fanny J. Sarrazin[1]

[1]Université Paris-Saclay, INRAE, UR HYCAR, 1 Rue Pierre-Gilles de Gennes, 92160 Antony, France
[2]Biostatistisc and Spatial Processes (BioSP), INRAE, Avignon 84914,France

Correspondence: Paul Zarpas (paul.zarpas@inrae.fr)

Abstract. Assessing long-term trends in irrigation water withdrawal (IWW) is essential for understanding the impacts of climate change on water resources and agricultural systems, yet long-term observations remain scarce. In France, annual IWW observations are only available from 2008 onward through the national water withdrawal database, limiting the analysis of long-term changes. To address this limitation, we develop a data-driven framework to reconstruct annual catchment-scale IWW over the 2000–2022 period. The approach relies on a generalized additive model (GAM), using structural (e.g., area equipped for irrigation) and hydro-meteorological (e.g., monthly mean temperature) predictors. The model explicitly identifies inter-catchment and inter-annual variability through a decomposition of total IWW into a base IWW term and a relative deviation term. The model is evaluated using a series of Leave-One-Period-Out cross-validation experiments. Results show robust predictive performance across all experiments (RMSE < 2 mm/yr) and reliable uncertainty estimates. The framework was then used to reconstruct annual IWW over the 2000–2007 period and to generate continuous time series of IWW at the catchment scale over 2000–2022. The reconstructed time series reveal widespread positive trends, with significant increases detected in 92% of catchments. Trend analysis indicates that changes in total IWW are primarily driven by the relative deviation component. A regional synthesis further identifies the Mediterranean region as a major hotspot, combining high IWW and strong IWW positive trends.

1 Introduction

The explicit representation of human influences on the water cycle in hydrological models is essential for assessing past, current and future water availability. This is required in particular for climate change impact assessment, in order to efficiently manage river basins and to inform climate adaptation public policies (Galelli et al., 2025; Kreibich et al., 2025). To integrate these influences into a hydrological modelling framework, the different uses of water have to be identified, described in terms of their temporal and spatial variabilities, and quantified. This often requires a substantial amount of field surveys, data collection and post-processing, which is a challenge even at the local scale (Santos et al., 2026; Vu et al., 2020).

Irrigated agriculture is a major water use that can significantly affect water availability (Puy et al., 2025; Yu et al., 2025), especially when its water demand peaks during summer low-flow periods (Mehta et al., 2024; Nie et al., 2021). Accurately estimating irrigation water withdrawal (IWW) volumes at large scales or within large-sample hydrological frameworks, how-

https://doi.org/10.5194/egusphere-2026-4287
Preprint. Discussion started: 17 August 2026

ever, presents several challenges (Puy et al., 2022b). Among them, we can cite the fragmented knowledge on actual local water use (e.g. irrigation practices, farmers decision calendars for irrigation, crop water requirements, artificial water storages), and the lack of long-term observational databases containing reliable information on where, when and how much water is withdrawn for irrigation to support IWW estimations and uncertainty quantification (Galelli et al., 2025). Accurate and temporally consistent estimates are nevertheless essential to support robust hydrological modeling (Nicolle et al., 2021; Thirel et al., 2015), and in general, to assess irrigation pressure on river system under changing climate and socio-economic conditions (Arboleda-Obando et al., 2025; Citrini et al., 2025; Tian et al., 2023).

In this context, modelling offers a valuable compromise for obtaining a coherent, complete, and continuous representation of irrigation dynamics across space and time (Linés and Werner, 2025; Portoghese et al., 2025). It allows to leverage existing knowledge to fill spatial and temporal data gaps where direct observations are missing (Dang et al., 2024; Gorguner and Kavvas, 2020). Modelling IWW is usually done through process-based or statistical models, and, in itself, presents its own challenges. Process-based models explicitly represent known energy and water fluxes as well as human decision-making processes (De Wit et al., 2019; Gaudou et al., 2014), but they present limitations as they often rely on poorly constrained parameters (Linga et al., 2025; Soutif-Bellenger et al., 2023; Puy et al., 2022a). In recent years, this limitation has stimulated the development of data-driven approaches for IWW estimation (Kragh et al., 2025; Zhang et al., 2025). In particular, the Random Forest (RF) algorithm, has shown strong performance in interpolation tasks, although it exhibits known structural limitations when used for extrapolation, i.e., when predicting beyond the conditions of its training sets (Muckley et al., 2023; Von Korff and Sander, 2022). This limitation has been highlighted by the difficulty of capturing interannual variability in IWW for a given catchment when temporal information is excluded from model training (e.g. a specific year) (Zarpas et al., 2026b). This can be explained by the fact that RF does not explicitly account for the spatiotemporal autocorrelation structure of IWW (Zarpas et al., 2026b).

Methodological developments are therefore needed to enable reliable temporal extrapolation of IWW by data-driven models. The relationship between IWW and its main predictors can be reasonably approximated by an additive structure (Zarpas et al., 2026b; Zhang et al., 2025). Under this assumption, additive models, such as the semi-parametric Generalized Additive Models (GAM, Hastie and Tibshirani, 1986), represent a promising way to perform extrapolation, as they mitigate the curse of dimensionality. GAMs provide smooth and continuous functional relationships and can naturally accommodate structured spatiotemporal effects. This is essential because data-driven IWW estimation from short reference time series, available on multiple sites, can be viewed as a spatiotemporal problem (Shortridge, 2023; Das et al., 2018), and particularly in the context of temporal extrapolation.

The objective of this study is to develop and evaluate a GAM based data-driven framework for the temporal extrapolation of annual IWW at the catchment scale, and to exploit the reconstructed time series to improve our understanding of long-term IWW dynamics. To do so, we extend the line of research we adopted in Zarpas et al. (2026b) by proposing a GAM-based framework for the temporal extrapolation of IWW and for extending annual IWW time series. The resulting temporally continuous IWW series enables subsequent time-series analyses, with trend assessment considered here as an illustrative application. To this end, we first assess the temporal extrapolation capability of the proposed GAM, using a demanding temporal cross-validation framework, while also quantifying prediction uncertainty. We then analyze IWW trends at the catchment scale.

https://doi.org/10.5194/egusphere-2026-4287
Preprint. Discussion started: 17 August 2026

The methodology is applied to the French national water withdrawal database (BNPE), which provides annual data from 2008 to 2022. It allows us to reconstruct continuous IWW time series over the 2000–2007 period. To produce IWW estimates, suitable for representing irrigated agriculture as a major anthropogenic influence on the water cycle, the analysis is carried out at the catchment scale over a dataset covering 498 catchments in France.

We present our methodology in Section 2, and the study area and data in Section 3. We then show the results in Section 4 and discuss them in Section 5, before concluding in Section 6.

2 Method

2.1 IWW decomposition

We propose a data-driven framework to extend in time a reference annual IWW database. Because the reference database spans numerous catchments and multiple years, two distinct sources of variability emerge: the inter-catchment variability and the intra-catchment inter-annual variability. Building on the decomposition proposed by Zarpas et al. (2026b), we decompose the total IWW (denoted as $\mathcal{W}_{y,c}$ for catchment c and year y) into 1) a structural component referred to as the base IWW term (denoted $\mathcal{W}^0_{y,c}$), representing the background level of IWW associated with long-term catchment characteristics and reference climatological conditions, while evolving over time through slowly varying anthropogenic predictors, and 2) an interannual component referred to as the relative deviation term (denoted $\delta\mathcal{W}_{y,c}$), describing year-to-year fluctuations from the structural level:

$$\mathcal{W}_{y,c} = \mathcal{W}^0_{y,c}\left(1 + \delta\mathcal{W}_{y,c}\right). \tag{1}$$

2.2 GAM set up

The spatio-temporal organization of the reference database has important implications for the GAM model formulation, as it induces a hierarchical dependence structure. In particular, some catchments are nested within others, inducing spatial correlation through shared drainage areas. The GAM formulation presented below is specifically designed to account for this hierarchical spatial dependence.

We model IWW in the logarithmic space to ensure strictly positive predictions of IWW, and to enable the identification of both the additive GAM decomposition and the multiplicative IWW variability decomposition of $\mathcal{W}_{y,c}$. We fit a GAM (f^{GAM}), using R package mgcv (Wood, 2011), as specified in Equation (2):

$$\log\left(\mathcal{W}_{y,c}\right) = f^{GAM}\left(\mathbf{X}_{y,c}\right) + \varepsilon_{y,c} = \sum_{i=1,..,n} f_i\left(x_{i,y,c}\right) + Z_c + \varepsilon_{y,c}, \tag{2}$$

where $\mathbf{X}_{y,c}$ is the predictor vector of individual component $x_{i,y,c}$; f_i is the individual smoother of the i-th component of the predictors, and n being the number of components of $\mathbf{X}_{y,c}$ and the summation running over all individual predictors; Z_c is a random effect - which introduces a hierarchical structure into the model (Pedersen et al., 2019); and $\varepsilon_{y,c}$ is the error, for the

https://doi.org/10.5194/egusphere-2026-4287
Preprint. Discussion started: 17 August 2026

year y and the catchment c. Spatial correlation is accounted for in the construction of the random effect (see Appendices A and B for details).

Since the predictor set $\mathbf{X}$ can be partitioned into predictors related to the IWW base term ($\mathbf{X}^0$) and to the relative deviation term ($\mathbf{X}^\delta$), the GAM can be rewritten as follows:

$$f^{\mathrm{GAM}}\left(\mathbf{X}_{y,c}\right) = \sum_{i=1,..,n^0} f_i^0\left(x_{i,y,c}^0\right) + \sum_{i=1,..,n^\delta} f_i^\delta\left(x_{i,y,c}^\delta\right) + Z_c, \tag{3}$$

where n^0 is the number of components of $\mathbf{X}_{y,c}^0$ and n^δ is the number of components of $\mathbf{X}_{y,c}^\delta$, and thus the sums are made on all individual predictors of the base term and of the relative deviation term, respectively. We note that in the log-space the IWW decomposition becomes:

$$\log\left(\mathcal{W}_{y,c}\right) = \log\left(\mathcal{W}_{y,c}^0\right) + \log\left(1 + \delta\mathcal{W}_{y,c}\right). \tag{4}$$

The identification between IWW components and the GAM decomposition thus provides the following estimators:

$$\begin{aligned} \log\left(\hat{W}_{y,c}^0\right) &= \textstyle\sum_{i=1,..,n^0} f_i^0\left(x_{i,y,c}^0\right) + Z_c, \\ \log\left(1 + \delta\hat{W}_{y,c}\right) &= \textstyle\sum_{i=1,..,n^\delta} f_i^\delta\left(x_{i,y,c}^\delta\right). \end{aligned} \tag{5}$$

2.3 Extrapolation evaluation: performance and uncertainty

2.3.1 Cross-validation experiment

To assess the ability of our model to produce reliable temporal extrapolation (here, on the 2000–2007 period) at the catchment scale, we perform temporal cross-validation experiments (Roberts et al., 2017) on the reference period (here, 2008–2022), where observations are available. Each experiment follows a Leave One Period Out (LOPO) strategy, in which the reference period is partitioned into blocks of consecutive years so that each block is in turn used as a test set for validation, while the remaining blocks form the training set. The length and, consequently, the number of time blocks used for validation varies from one LOPO experiment to another. We performed five experiments with 2, 3, 5, and 15 partitions of the reference period, respectively.

Specifically, we name LOPO2 the experiment where the reference 15-year period is partitioned in 2 sub-periods, one of 7 years and another of 8 years, both being alternately used as training and validation. In LOPO3, we have 3 sub-periods of 5 years each that are used for validation, with, every time, the remaining 10 years used for training. Finally, in LOPO5, we have 5 sub-periods of 3 years each used for validation, and, in LOPO15, we have 15 sub-periods of 1 year each (i.e., training is performed on 14 remaining years at each time). LOPO2 is then the experiment where the model is trained over the shortest period length, while in LOPO15 the model is trained over the longest period of data. It is to be noted that none of these experiments is a clear reference for our extrapolation over the 2000-2007 period (after training over the entire 2008-2022 period). However, altogether, this cross-validation strategy presents a continuum between an experiment that has a more representative extrapolation period length (in LOPO2, the validation length of 7-8 years is closer to the length of our 2000-2007 extrapolation period) and an experiment that has a more representative training period length (as in LOPO15, training is performed with 14 years out of the 15 years used in the extrapolation).

https://doi.org/10.5194/egusphere-2026-4287
Preprint. Discussion started: 17 August 2026

2.3.2 Metrics

The overall model performance is evaluated by considering all catchments pooled together, and by using the Root Mean Squared Error (RMSE) and the squared Pearson correlation coefficient r^2. Model performance is also evaluated at the catchment scale (i.e., on each catchment individually), using the predictive error normalized by the observed catchment mean. This Catchment Relative Error (CRE) is defined for a variable v estimated by $\hat{v}$ for a year y and catchment c as:

$$\mathrm{CRE}_{y,c} = \frac{v_{y,c} - \hat{v}_{y,c}}{\overline{v}_c}. \tag{6}$$

2.3.3 Uncertainty assessment

Uncertainties are modeled using the heteroscedastic log-normal distribution ($\mathcal{LN}^*$) detailed in Appendix D1, i.e. we consider the estimator of the IWW $\hat{\mathcal{W}}_{y,c}$ as:

$$\hat{\mathcal{W}}_{y,c} | \mathbf{X}_{y,c} \sim \mathcal{LN}^* \left(f^{GAM} \left(\mathbf{X}_{y,c} \right), \sigma^2_{y,c} \right). \tag{7}$$

The log-scale variance ($\sigma^2_{y,c}$), whose derivation is detailed in Appendix D2 accounts for two sources of predictive uncertainty: (i) a bias component, representing the irreducible prediction error associated with the adopted GAM formulation, i.e. the error that would remain even with an infinite amount of training data, i.e. a structural limitation of the model, and (ii) a prediction variance component, reflecting the uncertainty associated with estimating the GAM parameters from a finite training dataset. The bias is considered constant over time (y) and space (c) and the variance varies in time and space.

To assess the quality of this uncertainty estimation, we compare the nominal confidence level with the empirical coverage, i.e., the actual percentage of IWW data points contained within the confidence interval. This is performed for each cross-validation experiment.

To assess the spatiotemporal evolution of the prediction uncertainty, we synthesize its distribution for every prediction using CV, the coefficient of variation. It is defined as the ratio of the standard deviation of the uncertainty distribution (denoted $\sigma^{\mathcal{LN}^*}_{y,c}$) to the prediction (mean of the uncertainty distribution, denoted here $\mu^{\mathcal{LN}^*}_{y,c}$) :

$$\mathrm{CV}_{y,c} = \frac{\sigma^{\mathcal{LN}^*}_{y,c}}{\mu^{\mathcal{LN}^*}_{y,c}}. \tag{8}$$

Given the analytical form of the uncertainty distribution (Appendix D1 and Appendix D2), the coefficient of variation is reduced to an increasing function of the log-scale variance:

$$\mathrm{CV}_{y,c} = \sqrt{\exp\left(\sigma^2_{y,c}\right) - 1}. \tag{9}$$

To quantify temporal fluctuations around the average level of prediction uncertainty, we then define ΔCV, the deviation from the catchment mean CV (denoted $\overline{\mathrm{CV}}_c$ and computed over all years on the catchment c):

$$\Delta\mathrm{CV}_{y,c} = \mathrm{CV}_{y,c} - \overline{\mathrm{CV}}_c. \tag{10}$$

https://doi.org/10.5194/egusphere-2026-4287
Preprint. Discussion started: 17 August 2026

2.3.4 Time series visualization

To better visualize time series and facilitate comparison of the temporal evolution of IWW among catchments, we introduce the centered catchment-relative total IWW ($\mathcal{W}^{cr}_{y,c}$) and the centered catchment-relative IWW base term ($\mathcal{W}^{0,cr}_{y,c}$). These relative quantities remove the inter-catchment variability and highlight inter-annual variability within each catchment. This will enable the comparison between the actual relative deviation from the catchment mean and the identified (as per Equation (5)) relative deviation term, through the contribution of specific predictors, as per Equation (5). To this aim, the catchment-relative total IWW and the catchment-relative IWW base term are defined as:

$$\mathcal{W}^{cr}_{y,c} = \frac{\mathcal{W}_{y,c}}{\overline{\mathcal{W}}_c} - 1; \qquad \mathcal{W}^{0,cr}_{y,c} = \frac{\mathcal{W}^0_{y,c}}{\overline{\mathcal{W}^0}_c} - 1. \tag{11}$$

2.4 Trend analysis

2.4.1 Assessed variable

We assess the presence of a trend in IWW over the combined reference and extrapolation period (here 2000–2022) for each catchment, using the homogeneous and continuous time series produced by the model trained on all the available data in the reference period (here 2008-2022). We investigate potential trends in three quantities: the total IWW (predicted, $\mathcal{W}_{y,c}$), the IWW base term, $\mathcal{W}^0_{y,c}$, (identified from predictions - as per Equation (5)), and the relative deviation term, $\delta\mathcal{W}_{y,c}$, (identified from predictions- as per Equation (5)).

2.4.2 Catchment scale trend detection and quantification

For each of the three quantities presented in Sec. 2.4.1 - the trend assessment is conducted using the modified Mann–Kendall test (mMK) (Yue and Wang, 2004). This test is non-parametric and robust to outliers and accounts for temporal autocorrelation in the data. Among the detected trends, only the trends with a p-value below 0.05 are considered statistically significant. The strength of the trend is quantified using Sen's slope, a non-parametric estimator of the linear trend based on the median of pairwise slopes, which is robust to outliers (Sen, 1968). To improve interpretability and comparison across catchments, trend magnitude is expressed as a relative rate of change. It is computed by dividing Sen's slope by the catchment mean of the corresponding variable for total IWW and IWW base term (the relative deviation term is already dimensionless by construction). The resulting quantity is expressed in percentage per year (%/yr). The trend is denoted T_X for $X \in \left\{\mathcal{W}_{y,c}, \mathcal{W}^0_{y,c}, \delta\mathcal{W}_{y,c}\right\}$.

2.4.3 Regional trend indicators

To provide a regional-scale synthesis of the catchment trend analysis, we aggregate catchment-level trend of total IWW within major hydrographic regions. To do so, we construct a regional indicator of trend. For a region $\mathcal{R} = \{c_1, \ldots, c_{n_\mathcal{R}}\}$ containing $n_\mathcal{R}$ catchments of individual total IWW trend $\{T_{\mathcal{W},c_i}\}_{i \in 1, n_\mathcal{R}}$, we introduced the quantity $T_\mathcal{R}$, expressed in %/yr, defined as:

$$T_\mathcal{R} = \sum_i w_i T_{\mathcal{W},c_i}. \tag{12}$$

https://doi.org/10.5194/egusphere-2026-4287
Preprint. Discussion started: 17 August 2026

$T_{\mathcal{R}}$ is a weighted mean of the total IWW trends of individual catchments, with catchment-specific weights $\{w_i\}_{i=1,n_{\mathcal{R}}}$. The weights account for the redundancy induced by nested catchments, as detailed in Appendix C. A catchment involved in nested pairs will have a lower weight than a fully non-nested catchment. $T_{\mathcal{R}}$ is not intended to estimate the trend of aggregated regional IWW, but to summarize the diversity of catchment-scale trends within each region. We then define the unitless regional indicator of trend $I^T_{\mathcal{R}}$:

$$I^T_{\mathcal{R}} = \frac{T_{\mathcal{R}}}{\overline{|T|}}, \tag{13}$$

where $\overline{|T|}$ is the average over the regions of the absolute value of the $T_{\mathcal{R}}$ quantity.

To complement the regional trend indicator, we also construct a regional indicator of total IWW. We first introduced $\mathcal{W}_{\mathcal{R}}$ expressed in mm/yr, as:

$$\mathcal{W}_{\mathcal{R}} = \sum_i w_i \cdot \overline{\mathcal{W}}_{c_i}. \tag{14}$$

It is the analog of $T_{\mathcal{R}}$, but constructed with catchment mean total IWW (denoted $\overline{\mathcal{W}}_{c_i}$). The unitless IWW indicator $I^W_{\mathcal{R}}$ is then defined as:

$$I^W_{\mathcal{R}} = \frac{\mathcal{W}_{\mathcal{R}}}{\overline{|\mathcal{W}|}} \tag{15}$$

where $\overline{|\mathcal{W}|}$ is the average over the regions of the $\mathcal{W}$ quantity.

3 Case study

3.1 Study area and period

The study is conducted over 498 French continental catchments (Figure 1.a.1). Catchments were selected based on their size (catchment area larger than 350 km^2), and on the availability and quality of IWW data. We followed our previous study (Zarpas et al., 2026b) and we additionally excluded catchments until no pair of catchments exhibited a spatial correlation (ρ; defined in Appendix B) above 0.9. These catchments cover a wide range of agricultural and climatic conditions across France (Zarpas et al., 2026b; Delaigue et al., 2025a). Based on the French regional water agencies (organized around six metropolitan river basin districts), we defined eleven hydrological regions by regrouping subsets of catchments (Figure 1.a.1).

This study focuses on modeling IWW over the 2000-2022 period. IWW data are available from 2008 to 2022 - reference period for training and cross-validation (Figure 1.b). The 2000–2007 period corresponds to the temporal extrapolation period, for which IWW is to be reconstructed. Within the 2000-2022 period, a wide range of conditions are observed. For example, below-average temperature with above-average summer soil wetness (e.g. in 2002 or in 2014 and 2021, Figure 1.b), leading to below average IWW, as well as above-average temperature with below-average summer soil wetness (e.g. in 2003, or in 2019 and 2022, Figure 1.b), leading to above average IWW.

https://doi.org/10.5194/egusphere-2026-4287
Preprint. Discussion started: 17 August 2026

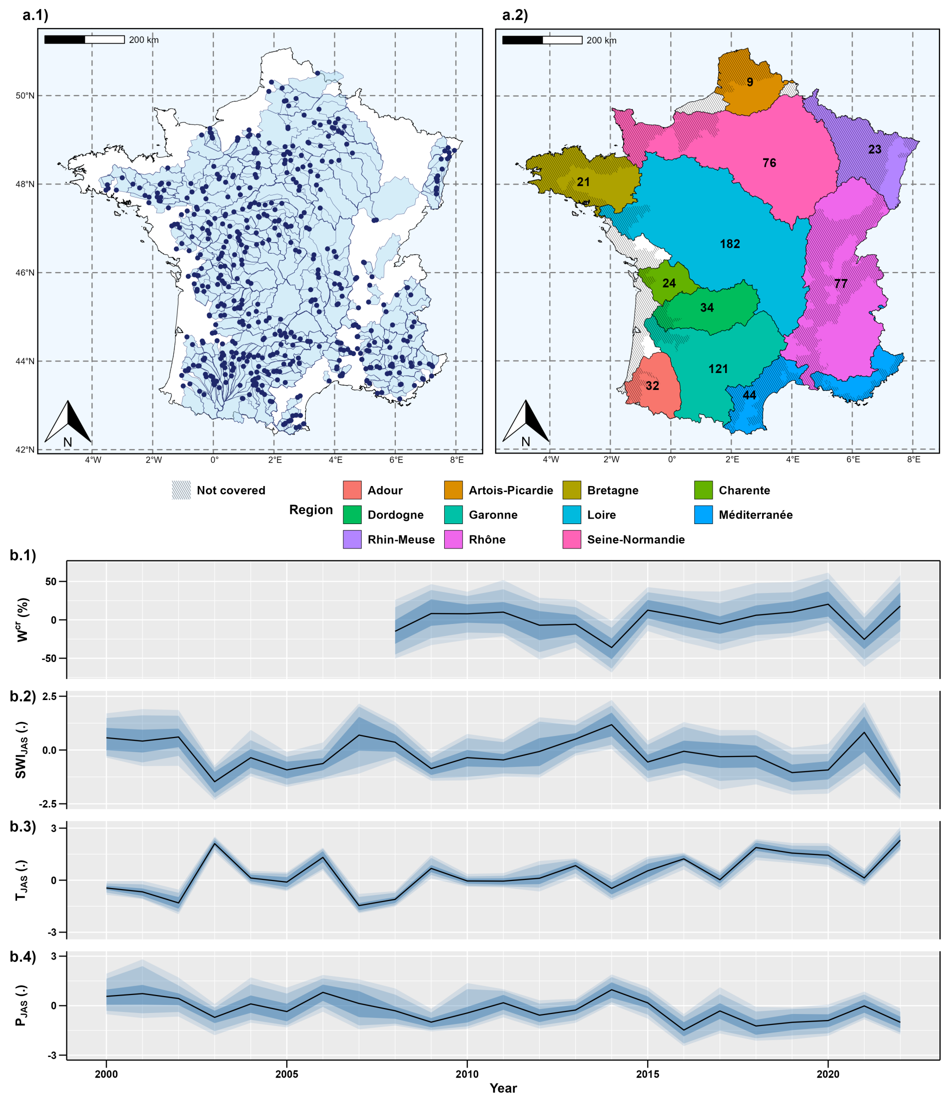

Figure 1. Presentation of the study area and data period. **a)** Maps of the study area with **a.1)** the selected catchments and **a.2)** their 11 corresponding hydrological regions (the number of catchments for each region is indicated, while hatched areas are not covered by the selected catchments). **b)** Evolution of the distribution across catchments of observed catchment-relative total IWW and summer (JAS) meteorological conditions through time (2000-2022). The shaded areas represent nested empirical quantile envelopes across catchments: the lightest band corresponds to the 5–95% range, the intermediate band to the 10–90% range, the darkest band to the interquartile range (25–75%). Panels show **b.1)** catchment-relative IWW and **b.2** to **b.4)** standardized summer meteorological variables, computed as deviations from the mean and divided by the standard deviation. Summer values are defined as the sum over July, August, and September. The variables shown are Soil Wetness Index (SWI), temperature (T), and precipitation (P).

https://doi.org/10.5194/egusphere-2026-4287
Preprint. Discussion started: 17 August 2026

3.2 Data

3.2.1 Irrigation Water Withdrawal

The French national water withdrawal database BNPE provides data obtained through compulsory declarations for any legal entity withdrawing an annual volume exceeding 10 000 m^3 (or 7 000 m^3 in some water-scarcity zones). IWW are geolocated, either at the actual withdrawal point or at the centroid of the associated municipality. In this study, data were aggregated at the catchment scale and annual volumes were converted to millimeters (mm/yr) within the catchment area. For some catchments, certain years are missing or excluded, due to unreliable data (Zarpas et al., 2026b). Therefore, the training dataset covers a total of 6799 points (i.e. 13.7 years per catchment on average - median: 15 years, 1st quartile: 12 years and minimum: 8 years).

3.2.2 Predictors

Predictors selection aims to maximize the GAM model in terms of predictive accuracy and interpretability (Marra and Wood, 2011). The predictor set used in this study builds upon the predictor importance analysis carried out in Zarpas et al. (2026b). While a large number of predictors may be relevant for IWW at the catchment scale, we choose to restrict the set of predictors in this study to reduce the complexity of the GAM model. Natural candidates include meteorological and hydrological conditions (e.g. temperature or precipitation, Nie et al., 2021; Lamb et al., 2021), agricultural-related variable (e.g. area equipped for irrigation (AEI), Zhu and Siebert, 2024; Lamb et al., 2021) and environmental conditions (e.g. hydrogeological context, Lamb et al., 2021). Finally, spatial information can also contribute substantially to explaining IWW variability (Zhang et al., 2025). Moreover, the interpretability of temporal extrapolation may be jeopardized by predictors that bring both temporal and spatial information (Van De Pol and Wright, 2009), particularly those that vary slowly over time but strongly across space (Wikle et al., 2019), such as crop types. This explains why we limited our study to Area Equipped for Irrigation (AEI) as agricultural predictor, which is widely regarded as the primary driver of irrigation (Shortridge, 2023; Zhang et al., 2022; Puy et al., 2021; Das et al., 2018).

The complete selection of predictors is presented in Table 1. Predictors are defined at the annual scale and at the catchment scale, i.e. each variable is associated with a given year y and catchment c. Meteorological predictors are derived from monthly variables standardized with respect to long-term averages for specific months. These monthly anomalies are aggregated at the annual scale for each year y and catchment c, so that they are annual predictors carrying infra-annual hydro-climatic conditions. We note that only AEI and meteorological predictors vary over time (i.e. from year to year), while all other predictors are time-invariant. As introduced in Sections 2.1 and 2.2, each predictor is associated with either the IWW base term or the relative deviation term. The IWW base term is primarily driven by static catchment attributes, with only limited temporal variation through AEI. In contrast, the relative deviation term is entirely driven by meteorological predictors. Because these predictors are expressed as deviations from a fixed climatic baseline (computed on the 1985-2015 period), the climatic signal is directly embedded in the relative deviation term. Finally, hydrogeological predictors are compositional, as they are constrained by a constant-sum condition within each catchment, which induces spurious correlations between components. To address this

https://doi.org/10.5194/egusphere-2026-4287
Preprint. Discussion started: 17 August 2026

issue, we apply an α-isometric log-ratio transformation (Clarotto et al., 2022). The parameter α is estimated by maximizing the log-likelihood, yielding $\alpha = 0.094$.

Table 1. Predictors used in this study

ID	Description	Type	Term	Source	Time dependent
AEI	Area equipped for irrigation (% of total catchment area)	Agricultural	$\mathbf{X}^0$	ELIAD$^{(1)}$	Yes (slowly)
T_aw	30-year average of temperatures for autumn-winter$^{(2)}$ (°C)	Environmental	$\mathbf{X}^0$	BDD-HydroClim$^{(3)}$	No
slope	Mean slope of the catchment (°)	Environmental	$\mathbf{X}^0$	CAMELS-FR$^{(4)}$	No
karstic	Percentage of catchment that is karstic (%)	Environmental	$\mathbf{X}^0$	CAMELS-FR$^{(4)}$	No
alluvial	Percentage of alluvial zones in the catchment (%)	Environmental	$\mathbf{X}^0$	CAMELS-FR$^{(4)}$	No
bedrock	Percentage of bedrock zones in the catchment (%)	Environmental	$\mathbf{X}^0$	CAMELS-FR$^{(4)}$	No
T_m	Mean monthly temperature normalized deviation from climatic average for the month $m^{(5)}$ (standardized, unitless)	Meteorological	$\mathbf{X}^\delta$	BDD-HydroClim$^{(3)}$	Yes
P_m	Total monthly precipitation normalized deviation from climatic average for the month $m^{(6)}$ (standardized, unitless)	Meteorological	$\mathbf{X}^\delta$	BDD-HydroClim$^{(3)}$	Yes
SWI_m	Mean monthly soil wetness index normalized deviation from climatic for the month $m^{(7)}$ (standardized, unitless)	Meteorological	$\mathbf{X}^\delta$	BDD-HydroClim$^{(3)}$	Yes

$^{(1)}$: Zhu and Siebert (2024), $^{(2)}$: climatic baseline years are 1985-2015, $^{(3)}$: Delaigue et al. (2025b) (https://webgr.inrae.fr/eng/tools/databases/bdd-hydroclim), $^{(4)}$: Delaigue et al. (2025a), $^{(5)}$: selected months for temperature: July, August $^{(6)}$: selected month for precipitation: July, $^{(7)}$: selected months for soil wetness index: July, August, September.

4 Results

4.1 Model evaluation

4.1.1 Prediction performance

Figure 2 presents the results of the cross-validation experiments on total IWW. Figure 2.a) shows the scatter plots of predictions versus observations for each of the four temporal cross-validation experiments – namely LOPO2, LOPO3, LOPO5, and LOPO15 (see Section 2.3.1), considering all catchments together. Figure 2.b) presents the violin plots of the catchment relative error (CRE) for each experiment, illustrating performance at the catchment scale.

The results show that the model achieves high performance across all experiments. The overall evaluation shows that r^2 values never fall below 0.92 and RMSE values never rise above 1.95 mm/yr (Figure 2.a). At the catchment scale, the magnitude

https://doi.org/10.5194/egusphere-2026-4287
Preprint. Discussion started: 17 August 2026

of the CRE (being positive or negative) remains below 30% for 82% (LOPO15), 81% (LOPO5), 78% (LOPO3) and 73% (LOPO2) of the total number of predictions (Figure 2.b). The violin plots show that errors are relatively well centered and symmetric around zero. Some extreme positive errors are, however, observed, especially for LOPO2 (0.8 % of points) where the absolute CRE exceeds 100%. When looking at the high CRE values in details, we observed that most cases (79 % of occurrences) concern IWW values below 1 mm/yr, for which relative errors become unstable due to small denominator values, which explains high CREs.

Model performance slightly degrades for LOPO2 (mostly in terms of extreme CRE values), but the model remains stable in temporal cross-validation experiments (Figure 2.a). Overall, the model performs very similarly across experiments, despite their increasingly challenging cross-validation conditions in terms of reduced training information and longer testing time block length.

4.1.2 Uncertainty estimation

Figure 3 presents the performance of uncertainty estimation for each cross-validation experiment. We can see that the uncertainty estimates cover a percentage of observations that closely matches the expected coverage across confidence levels. The actual and nominal coverages exhibit r^2 values above 0.99 for each LOPO experiment, illustrated by the curves close to the straightline in Figure 3. The uncertainty estimates exhibit some miscoverages. However the maximum difference between expected and empirical remains below 5% for LOPO3 (undercoverage) and for LOPO5 and LOPO3 (overcoverage), while LOPO 2 is the experiment where the estimates perform worst, with maximum undercoverage of 9%. Despite these difference, overall, the uncertainty estimation performs consistently well across the cross-validation experiments.

4.2 IWW prediction and uncertainty

The output of the final IWW prediction model (i.e. the model trained on all the available data) is presented for the total IWW (Figure 4.a) and its identified components: the relative deviation term ($\delta\mathcal{W}$, Figure 4.b)) and the IWW base term ($\mathcal{W}^0$, Figure 4.c). To focus on inter-annual variability, and remove intercatchment variability, we consider the catchment-relative total IWW and IWW base term, as defined in Section 2.3.4. The prediction period covers 2000-2022

We observe that the inter-annual variability of the total IWW closely mirrors that of the relative deviation term, both in amplitude and temporal pattern. More precisely, a very strong and consistent temporal coherence is observed between total IWW and the relative deviation term, across all catchments, with Pearson correlation coefficients exceeding 0.91 in all cases (median: 0.99). This indicates that the inter-annual variability in the total IWW (W) is almost entirely governed by the relative deviation term ($\delta\mathcal{W}$).

In contrast, the IWW base term component $\mathcal{W}^0$ exhibits a markedly narrower inter-annual spread and a smoother temporal pattern. In addition, the IWW base term (W^0) shows consistently high lag-1 autocorrelation (median: 0.86), indicating a strong temporal persistence and a slowly evolving system in time. By contrast, both the total IWW (W) and the deviation term (δW) exhibit near-zero lag-1 autocorrelation (medians of 0.05 and 0.06, respectively).

https://doi.org/10.5194/egusphere-2026-4287
Preprint. Discussion started: 17 August 2026

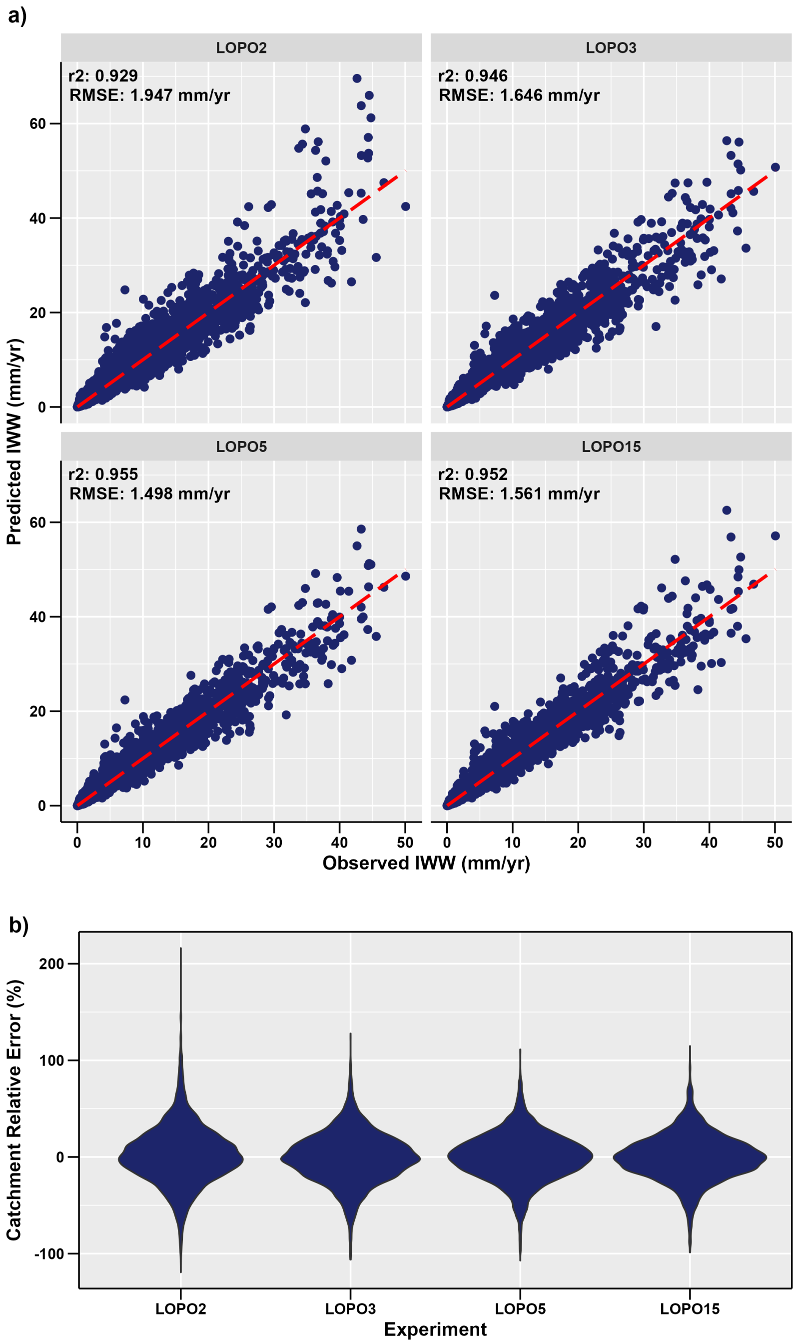

Figure 2. Cross-validation experiments (LOPO2, LOPO3, LOPO5 and LOPO15), presented in Section 2.3.1 : **a)** Scatter plots of predictions versus observations, with r^2 and RMSE indicated for each experiment and **b)** Violin plots of Catchment Relative Error.

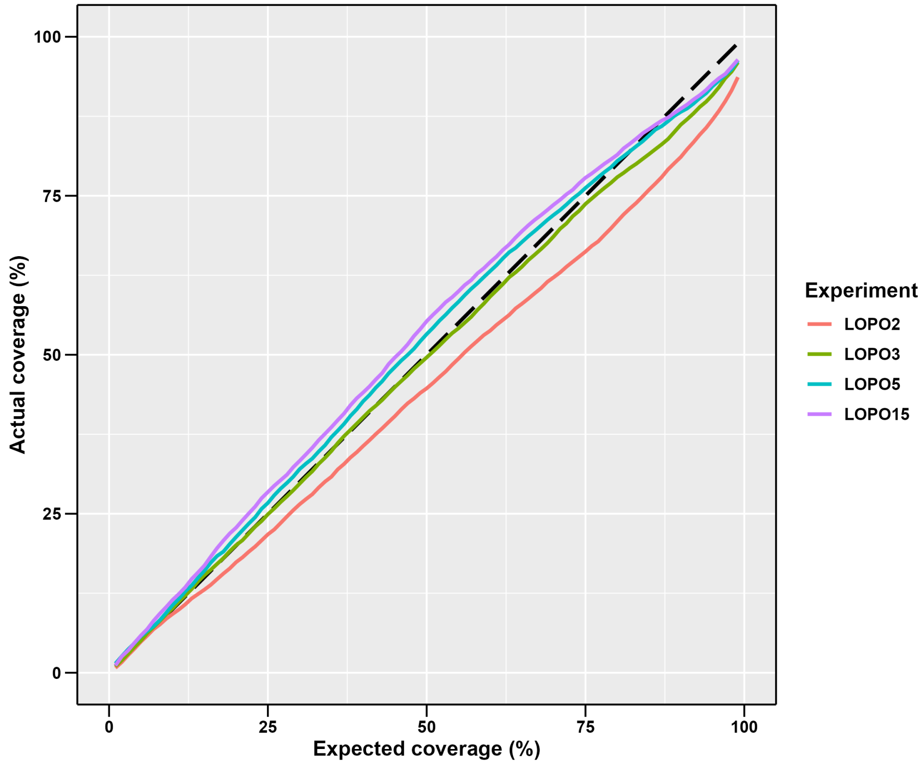

Figure 3. Uncertainty estimation performance: actual coverage vs. expected coverage across confidence levels for all cross-validation experiments.

Beyond the distribution of inter-annual IWW variability across the identified components, the model captures high values of total IWW for the period 2003–2005, with these anomalies being primarily reflected in the relative deviation term component. In addition, both the catchment-relative total IWW and the relative deviation term exhibit a tendency toward higher values during the most recent period (approximately 2015–2022), with the exception of 2021, suggesting a potential shift in recent hydro-climatic conditions (see Section 4.4 for the trend analysis).

Figure 5 illustrates the model uncertainty, evaluated through the coefficient of variation CV, defined in Section 2.3.3. Figure 5.a) displays the cumulative distribution of CV across all predicted points (498 catchments, 22 years), demarking points inside and outside the training set (points spanning over the 2008-2022 period). Figure 5.b) shows the temporal evolution of the distribution of ΔCV, defined in Section 2.3.3, across catchments.

https://doi.org/10.5194/egusphere-2026-4287
Preprint. Discussion started: 17 August 2026

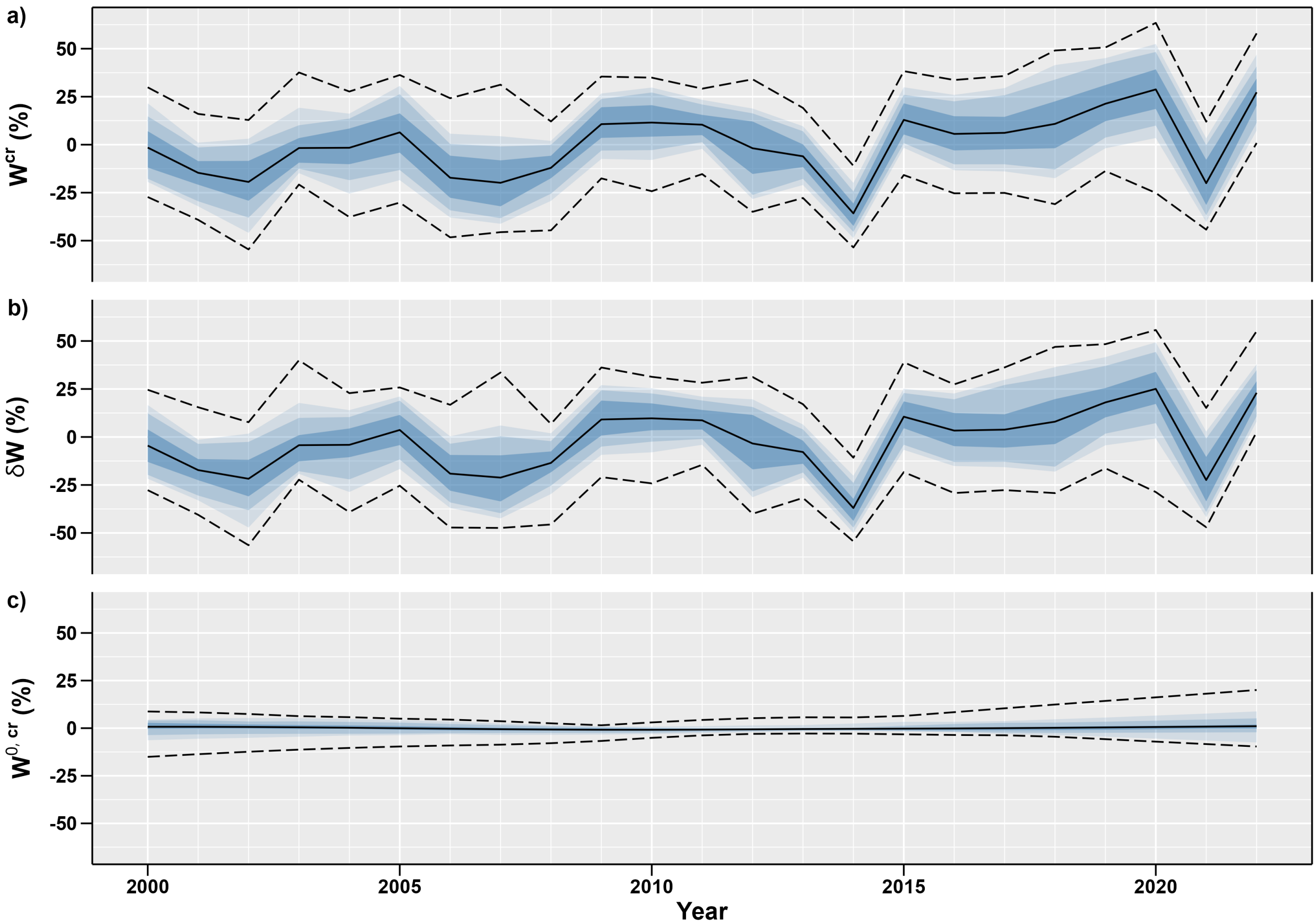

Figure 4. Evolution of the distribution of predicted IWW and its identified components across catchments and through time. The shaded areas represent nested empirical quantile envelopes across catchments: the lightest band corresponds to the 5–95% range, the intermediate band to the 10–90% range, the darkest band to the interquartile range (25–75%), the dotted lines indicate the full range of predicted variability (minimum and maximum across catchment) and solid lines represent the mean across catchment. Panels show **a)** the catchment-relative total IWW ($\mathcal{W}^{cr}$), **b)** the relative deviation term ($\delta\mathcal{W}$) and **c)** the catchment-relative IWW base term ($\mathcal{W}^{0,cr}$).

We observe that the CV exhibits limited variability: all values range between 23.8 % and 29.8 %, while 97.5% of CV points fall between 23.8% and 25%. Differences can be observed between the distribution of CV from points inside and outside the training set, although they remain small (mean CV of 24 % for points inside training set and 24.2 % for those outside).

When looking at CV variability in time (through ΔCV as defined in Section 2.3.3), we observe that extrapolated years (2000-2007) are more uncertain. The extrapolated years exhibit higher mean and 75th percentile of ΔCV, and thus higher prediction uncertainty, than the reference period (2008-2022). This increase is particularly pronounced for years such as 2003 and 2006, as shown in Figure 5. However, high CV values appear to be driven primarily by catchment-specific uncertainty

https://doi.org/10.5194/egusphere-2026-4287
Preprint. Discussion started: 17 August 2026

rather than inter-annual variability. This is supported by the distribution of catchment-mean CV (as defined in Section 2.3.3), which exhibits a standard deviation of 0.64%, exceeding the maximum temporal deviation in CV (ΔCV).

We note that the uncertainty associated with the GAM prediction variance component (as described in Section 2.3.3) represents only a small fraction of the total predictive uncertainty log-variance. Over the 2000–2022 period, the ratio between the prediction variance the total predictive uncertainty log-variance has a median of 0.07 and a 75th percentile of 0.09 (not shown).

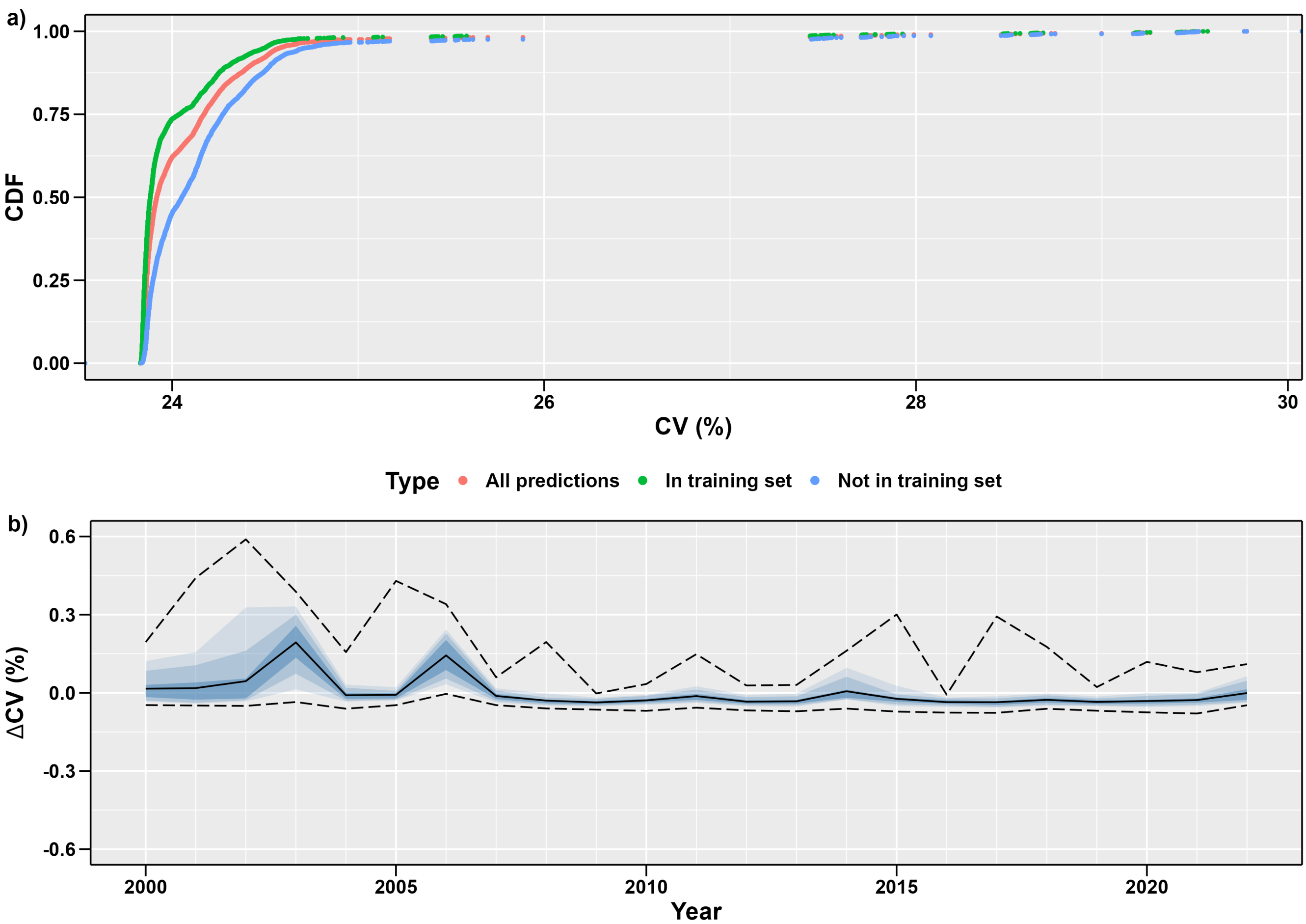

Figure 5. Values of the prediction coefficient of variation (CV). **a)** Cumulative distribution function for individual predictions and catchment means. **b)** Evolution of the distribution across catchments of ΔCV: the shaded areas represent nested empirical quantile envelopes across catchments: the lightest band corresponds to the 5–95% range, the intermediate band to the 10–90% range, the darkest band to the interquartile range (25–75%), the dotted lines indicate the full range of predicted variability (minimum and maximum across catchments) and solid lines represent the mean across catchments.

https://doi.org/10.5194/egusphere-2026-4287
Preprint. Discussion started: 17 August 2026

4.3 Interpretation of the fitted smoother GAM

To gain insight into the relationships learned by the GAM and assess their interpretability, we examine the fitted smoothers associated with each time-varying predictors (Figure 6). The effect of AEI on the IWW base term is positive and nearly linear in the log-space. Most meteorological predictors display near-monotonic responses, with soil moisture exhibiting a decreasing relationship with the relative deviation term. More complex responses are observed for a limited number of predictors, notably July precipitation and August temperature, where the fitted smoothers display localized non-monotonic behaviour at the extremes of the predictor range.

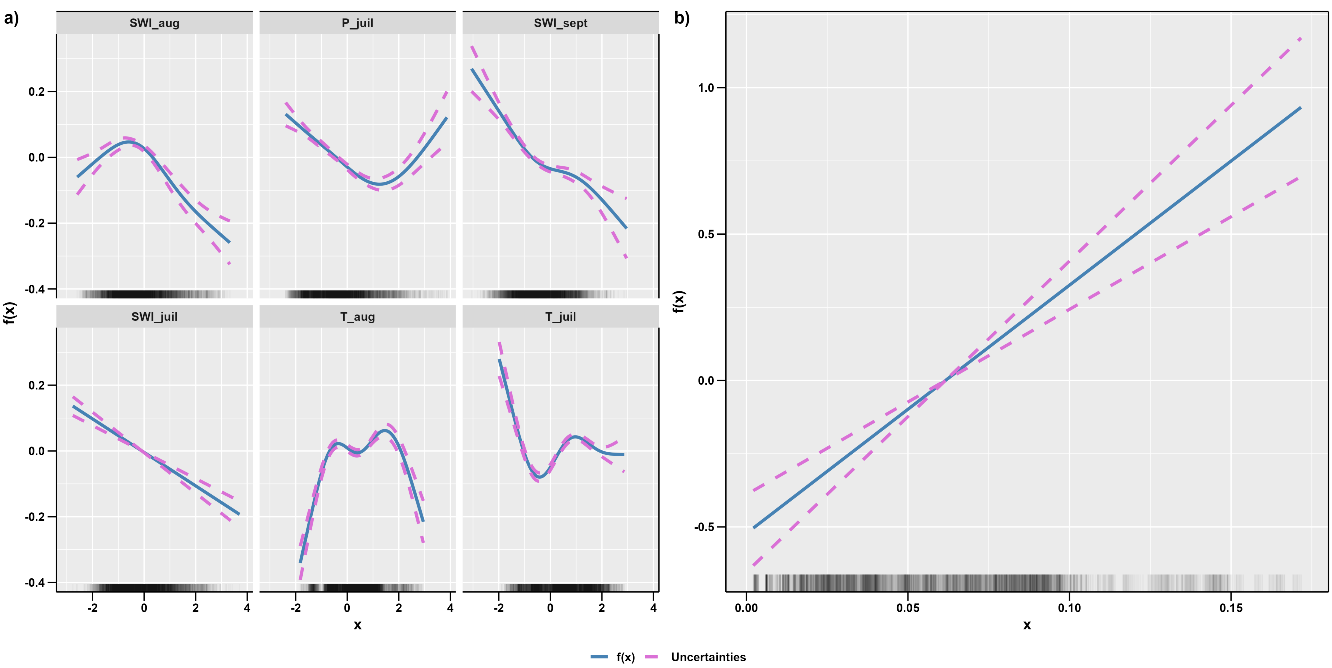

Figure 6. Fitted smoothers of **a)** the hydrometeorological predictors associated with the relative deviation term and **b)** the Area Equipped for Irrigation (AEI), associated with the IWW base term. Solid blue lines denote the estimated smoothers and dashed purple lines the associated 95% confidence intervals. Rugs along the horizontal axis indicate the distribution of the observations used for model fitting.

4.4 Trend

4.4.1 Trends at the catchment scale

Catchment-scale trends were calculated and tested for statistical significance as described in Section 2.4.2. Results shown in Figure 7.a present a map of these significant trends, for total IWW (7.a.1), IWW base term (7.a.2) and the relative deviation term (7.a.3). Results shown in Figure 7.b) present the corresponding histogram of the magnitude of the significant trend, for

https://doi.org/10.5194/egusphere-2026-4287
Preprint. Discussion started: 17 August 2026

total IWW (7.b.1), IWW base term (7.b.2) and the relative deviation term (7.b.3). Significant trends are detected in 92%, 62% and 96% of the total number of catchments, respectively for the total IWW, the IWW base term, and the relative deviation term.

The detected significant trends are essentially positive for the total IWW (only one significant negative trend), and the relative deviation term (all significant trends are positive). In contrast, the detected significant trends of the IWW base term are more evenly distributed (44% positive and 56% negative). Results show that most of the magnitude of the significant trends in the total IWW and in the relative deviation term exceed 0.75%/yr (80% and 85% of the catchments, respectively), while a substantial fraction also exceed 1.5%/yr (33% and 28% of catchments, respectively). In contrast, the magnitude of the trends detected for the IWW base term are mostly between $-0.20\%/\text{yr}$ and $0.20\%/\text{yr}$ (52% of the catchments), and they seldom exceed 1.5%/yr (0.64% of catchments).

Significant and positive trends for the total IWW and the relative deviation term are widespread across France (the only negative trend – for total IWW – is in Charente, southwestern France). However, spatially coherent patterns can be identified, with particularly strong signals in catchments located in the central (Loire and Dordogne) and eastern (Rhin–Meuse) regions for both the total IWW and the relative deviation term, and a strong signal in the north (Artois-Picardie) region for the total IWW. Significant trends for the IWW base term also exhibit spatially coherent patterns, with positive trends in the north (Artois–Picardie) region and negative trends in parts of southwestern France (Loire and Charente catchments) region.

4.4.2 IWW base term and relative deviation term influence on total IWW

In this section, we present the results on the respective influence of the IWW base term and the relative deviation term on the total IWW trend (Figure 8). Figure 8.a presents the proportion of catchment for different configuration of direction and significance of the trend across the term. This configuration is summarized in a trend state, which is symbolized by ↑ if a significant trend is detected, by ↓ if a negative trend is detected and by • if no significant trend is detected. The combinations across terms is simply the concatenation ($\mathcal{W}, \mathcal{W}^0, \delta\mathcal{W}$) of the trend state of each state. Figure 8.b then presents the comparison of the trend magnitude for each term.

The distribution of trend state combinations indicates that the total IWW trends are primarily driven by the relative deviation term trends. In 92% of the catchments, both the total IWW and the relative deviation term exhibit significant positive trends, regardless of the IWW base term trend state. However, some compensating effects are observed: negative trends in the IWW base term can offset positive trends in the relative deviation term (3% of catchments, mostly located in the Charente region. In rarer cases – combination (↑,↑,•) and (↓,↓,•), the total IWW trends are instead driven by the IWW base term (1.2% of catchments, located in Brittany, Loire, and Charente).

Comparing trend magnitude for the IWW base term and the relative deviation term (Figure 8.b) reveals that these two terms largely carry independent information, as indicated by their low Pearson correlation (0.17). These two terms are associated to the trend magnitude of the total IWW term, as the Pearson correlation between the trend magnitude of the total IWW and the IWW base term is 0.63 and the Pearson correlation between the trend magnitude of the total IWW and the relative deviation term is 0.87. The magnitude of the total IWW trends is primarily driven by the relative deviation term: in 80% of catchments, the ratio between the trend magnitude of the total IWW and the relative deviation term exceeds 0.8. However, a modulation

https://doi.org/10.5194/egusphere-2026-4287
Preprint. Discussion started: 17 August 2026

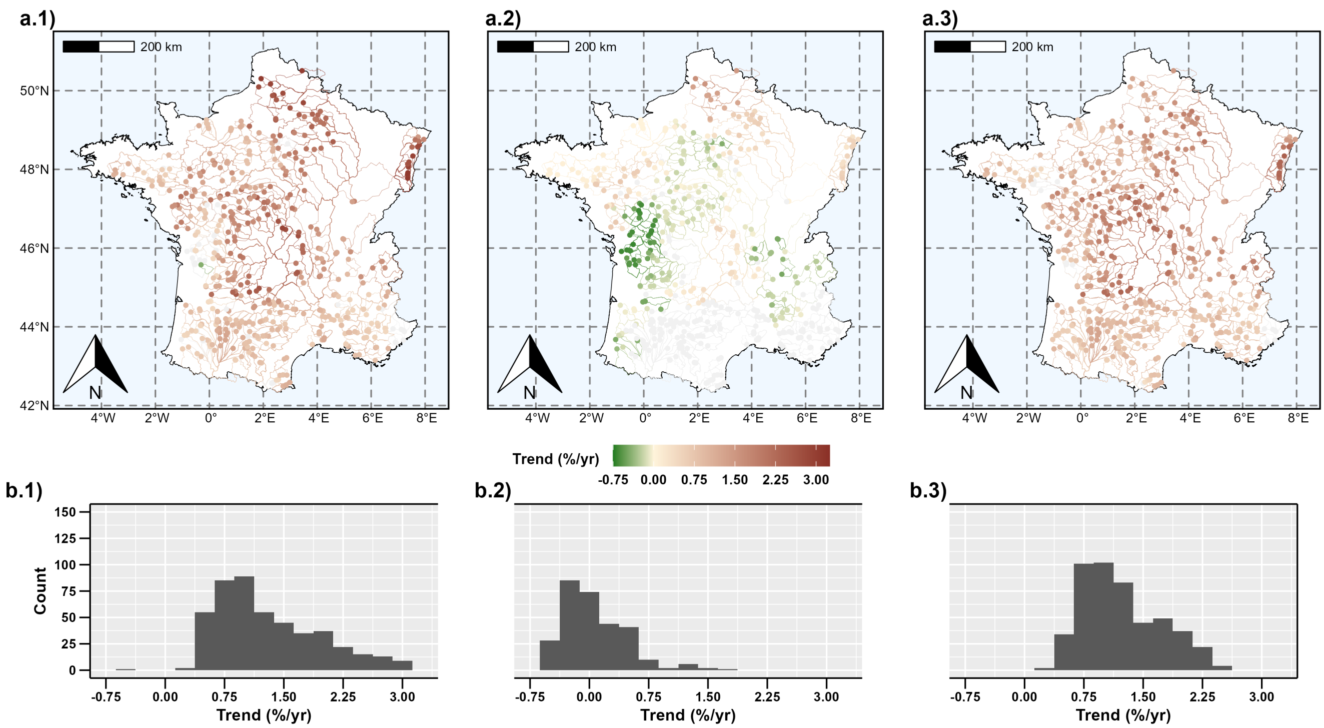

Figure 7. Magnitude of estimated trends at the catchment scale. **a)** Maps of the trend (gray indicates absence of significant trend) for **a.1)** the total IWW ($\mathcal{W}$), **a.2)** the IWW base term ($\mathcal{W}^0$) and **a.3)** the relative deviation term ($\delta\mathcal{W}$). **b)** Histogram of trend magnitude for **a.1)** the total IWW ($\mathcal{W}$) (463 catchments with trends), **a.2)** the IWW base term ($\mathcal{W}^0$) (310 catchments with trends) and **a.3)** the relative deviation term ($\delta\mathcal{W}$) (479 catchments with trends).

effect from the IWW base term is also highlighted: for a given range of relative deviation term trend magnitude, the total IWW trends vary according to the IWW base term trend magnitude (when moving from left to right). This modulation can, in some cases, lead to amplification effects. For example, in northern catchments (Seine river basin and Artois–Picardie), strong positive trends in both the IWW base term and the relative deviation term (between 1 and $1.5\%/\text{yr}$ for each) result in particularly large total IWW trends (exceeding $2.5\%/\text{yr}$).

4.4.3 Regional synthesis of total IWW trends

Figure 9 presents the regional indicators of trend (Figure 9.a), which are put into perspective with the regional indicators of total IWW (Figure 9.b). Both indicators are obtained by aggregating catchment-scale information, as described in Section 2.4.3, within each hydrographic region, as presented in Section 3.1. Regional trend indicators (I^T) are positive in all regions except Charente. Values range from -0.51 to 1.85 (Artois-Picardie), with a median of 0.86 (Figure 9.a)). The comparison between I^T and I^W highlights marked differences between regional indicators of IWW and trend. In particular, Adour, the

https://doi.org/10.5194/egusphere-2026-4287
Preprint. Discussion started: 17 August 2026

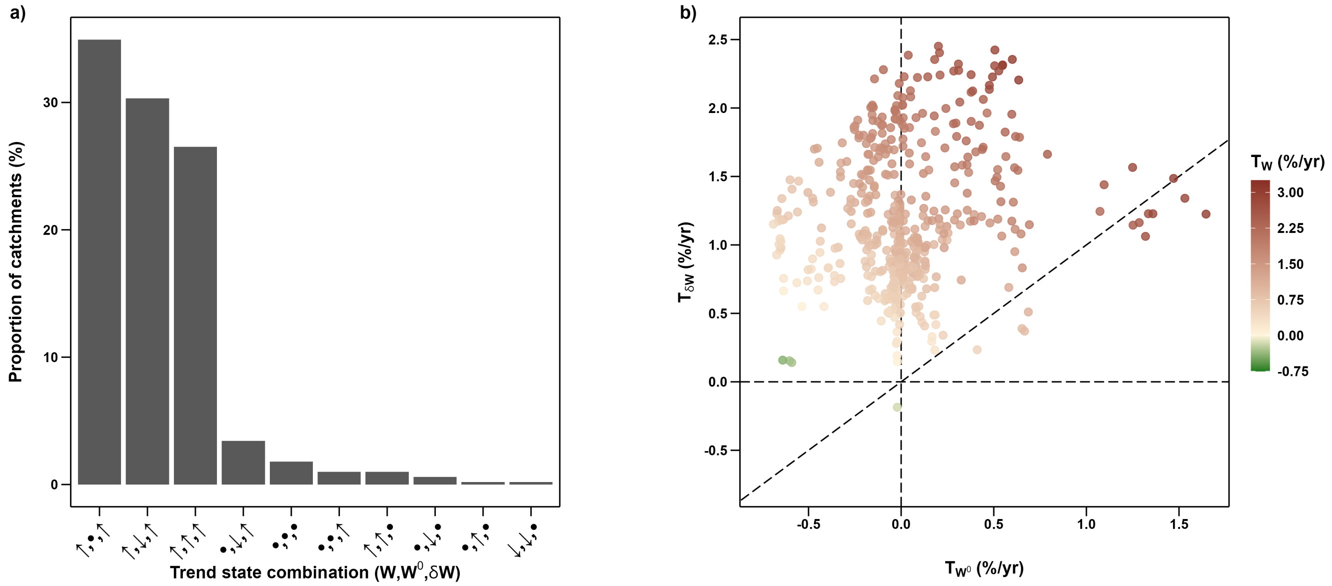

Figure 8. Comparison of trend behavior among the total IWW ($\mathcal{W}$), the IWW base term ($\mathcal{W}^0$) and the relative deviation term ($\delta\mathcal{W}$). **a)** Bar plot showing the proportion of catchments exhibiting each combination of trend states across term. **b)** Scatter plot of trend magnitude for the relative deviation term versus the IWW base term, with the strength of the total IWW trend shown using a color scale.

most irrigated region (I^W of 2.72), exhibits only moderate trend values (I^T of 0.57), while Mediterranean region combines the second strongest trend indicator (I^W of 1.84) with the second strongest IWW indicator (I^T of 1.58).

5 Discussion

5.1 Modeling approach and temporal extrapolation

Our model demonstrates strong predictive performance across all leave-one-period-out (LOPO) experiments, indicating robust temporal extrapolation capabilities (Figure 2). However, errors can be non-negligible when looking specifically at the individual catchment scale, with a limited number of extreme prediction errors (i.e. when CRE > 100%), particularly in the LOPO2 experiment, where cross-validation is performed over only two long periods (7 and 8 years). Those extreme LOPO2 relative errors can come from either the reduction of the length of the training set, or from the increase of the length of the testing set. Despite these observed extreme LOPO2 errors, the temporal evolution of catchment-relative total IWW prediction remains stable and acceptable over the extrapolation period (2000–2007), with no abrupt temporal changes or unrealistic spatial patterns detected in the reconstructed time series (Figure 4) or in the detected trends (Figure 7). This suggests that the degraded performance observed in the LOPO2 experiment is more likely attributable to the reduced size of the training dataset than to

https://doi.org/10.5194/egusphere-2026-4287
Preprint. Discussion started: 17 August 2026

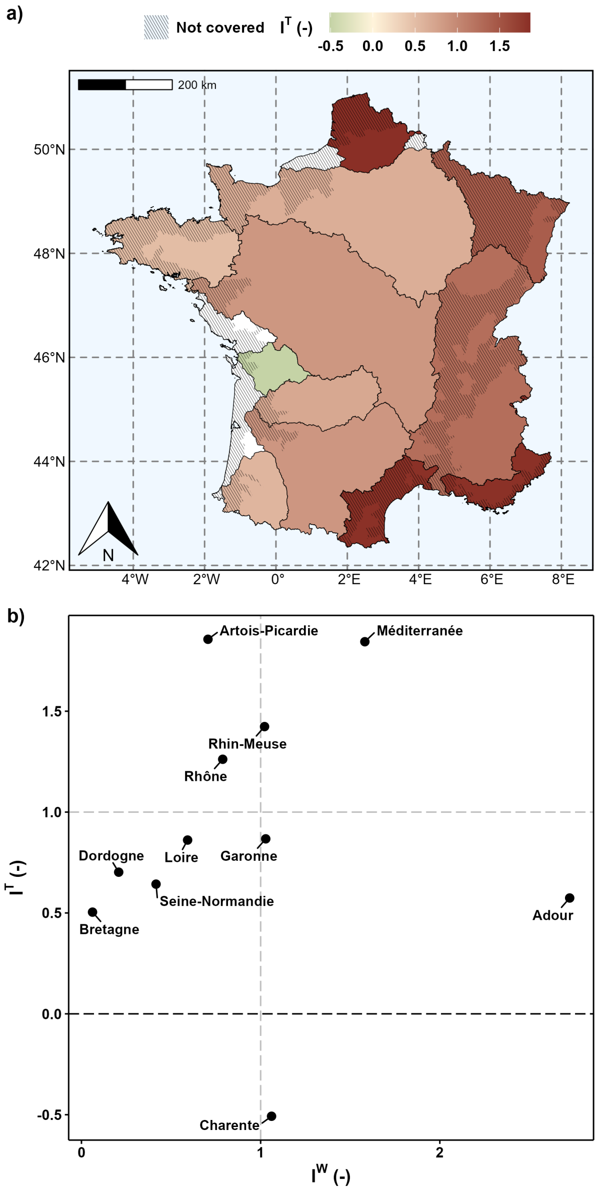

Figure 9. Regional indicators of trend and total IWW. **a)** Map of regional indicator of trend (I^T) in the 11 hydrographic regions defined in Section 3.1. **b)** Relationship between the regional indicators for the total IWW (I^W) and the indicator for trend (I^T). Region labels correspond to the major French hydrographic regions (Figure 1). The black dashed horizontal line separates negative and positive regional trend indicators. Gray dashed horizontal and vertical lines separate above and below average the positive regional trend indicators and regional IWW indicators, respectively.

https://doi.org/10.5194/egusphere-2026-4287
Preprint. Discussion started: 17 August 2026

an increased extrapolation horizon, a known pitfall when temporal coverage is restricted (Roberts et al., 2017). This limitation of the LOPO2 experiment may also explain the slight undercoverage observed in our uncertainty estimates.

Overall, our uncertainty estimation produces credible prediction intervals, providing further confidence that our extrapolation is both reliable and consistently evaluated. However, this uncertainty framework relies on the assumption that model bias remains constant over time, particularly under temporal extrapolation (i.e we work under the assumption that the structural limitation of our model remain constant). Such an assumption may lead to the underestimation of uncertainty and highlights the need for further refinement of the uncertainty estimation framework to better account for potential time-varying model biases (see e.g. Hsueh et al., 2024).

Beyond predictive performance, the model identifies three years with high IWW in the 2000-2007 period: 2003, 2004 and 2005, which are known to be drought years (Amigues et al., 2006). Moreover, the model successfully recovers meaningful structural components of IWW; namely the IWW base term and the relative deviation term. In particular, the decomposition into IWW base term and relative deviation term components emerges naturally from the semi-parametric structure of the model, without explicit supervision, highlighting the relevance of this formulation. This decomposition is consistent with the nature of the predictors, with low-frequency variability (e.g. AEI) primarily associated with the base component, while high-frequency meteorological variability drives the relative deviation term of the modeled IWW.

The fitted smoothers are generally consistent with physical expectations (Figure 6), supporting the interpretability of the proposed decomposition. The effect of AEI suggests that base IWW increases approximately proportionally with the equipped irrigated area, which is consistent with the literature (Puy et al., 2021). The effect of meteorological predictors suggests, overall, lower IWW under wetter conditions and higher IWW under dryer conditions, which is also consistent with the literature (Nie et al., 2021). A limited number of predictors display less intuitive responses under extreme conditions (e.g. P_juil or T_aug). These localized behaviors should be interpreted cautiously, as the smoothers represent partial effects estimated under the adopted additive formulation and are less constrained in sparsely sampled regions of the predictor space. Future work could investigate whether incorporating selected interactions or additional physical constraints could further improve the interpretability of these relationships.

Our model uncertainty appears to be driven primarily by the bias, which dominates the prediction variance. This corresponds to a situation of systematic over-smoothing, which is relatively uncommon in modern machine learning applications (Marra and Wood, 2012). Given the performance observed in temporal cross-validation, this suggests that the model is stable but eventually oversimplified. We propose two possible explanations for this behavior. First, the model lack of predictors such as crop type or irrigation practices, which could improve local predictive capacity. It must be noted that some variables were intentionally excluded (crop type) to improve extrapolation interpretability (Section 3.2.2), as they primarily encode spatial rather than temporal variability (Van De Pol and Wright, 2009), while others are simply unavailable at the catchment or annual resolution (e.g. detailed agricultural practices), despite their known importance for IWW estimation (Kragh et al., 2025; Soutif-Bellenger et al., 2023). Second, the training data themselves are likely affected by substantial noise. This concerns both the predictors, which are not always available at the appropriate spatial scale, and the target variable, as the reference IWW dataset (here,

https://doi.org/10.5194/egusphere-2026-4287
Preprint. Discussion started: 17 August 2026

the BNPE) estimates may contain uncertainties related to reporting procedures inherent to mandatory declaration systems, as suggested for similar administrative water-use datasets (Sangha and Shortridge, 2023).

Taken together, these limitations suggest that further research could focus on improving the quality, consistency, and representativeness of the training dataset. Overall, our findings reflect a classical accuracy–robustness trade-off, previously discussed in other machine learning contexts (Zhang et al., 2019; Tsipras et al., 2019), and suggest potential avenues for improving the prediction model in future work.

5.2 Trend assessment

The decomposition of total IWW into a base IWW term and a relative deviation term provides insight into the underlying processes. Trends in the relative deviation term are spatially coherent and align well with documented climatic changes in France, including increasing temperatures (Ribes et al., 2022; Twardosz et al., 2021), decreasing summer soil water content (Almendra-Martín et al., 2022; Řehoř et al., 2024), and declining summer precipitation (Haruna et al., 2026). In particular, these studies are consistent with the trends detected in the relative deviation term (i.e. the term in our model that carries the climatic signal), and with their spatial distribution, particularly in hotspot regions, such as central and eastern France. These results support the interpretation of the identified relative deviation ($\delta\mathcal{W}$) in our model as a proxy for climate-driven variability in IWW. In contrast, trends in the identified (IWW base term $\mathcal{W}^0$) are generally weaker and may be either positive or negative. This can be directly attributed to the fact that AEI is the only time-varying predictor of the IWW base term (with a positive linear effect in log-space, Figure 6), and AEI itself exhibits this behavior (Zhu and Siebert, 2024). The detected spatial patterns are also consistent with national reports, which identify similar hotspots of irrigation evolution, including Charente and Artois–Picardie (Sédillot et al., 2024). Although the contribution of the IWW base term to detected trends in our study is comparatively limited, recent national assessments suggest that changes in agricultural practices and irrigation development may play an increasing role in future irrigation dynamics (Arambourou and Ferrière, 2025).

Although long-term trends in total IWW have not been extensively documented in France, the widespread positive trends observed in the relative deviation term component are consistent with the expected increase in crop water demand under climate change on the worldwide literature (Warziniack et al., 2022; García-Garizábal et al., 2014; Döll, 2002). While trends in the total IWW are largely driven by the relative deviation term (i.e. by the climatic signal), the IWW base term also plays a role and provides contrast to the climatic signal. The decomposition into a IWW base term and a relative deviation term that we adopted in our framework, and the results obtained from its application in France, suggest that the temporal dynamic in IWW cannot be interpreted solely as a direct response to climate, which also has been previously highlighted in the literature (Warziniack et al., 2022; Zhang et al., 2022; Puy et al., 2021). Variations in structural variables (in our case, AEI) should also be considered in long-term analyses.

The regional indicators of trend provide a complementary perspective to the catchment-scale analysis by synthesizing trends at the scale of major hydrographic regions. Unlike computing trends from region-wide aggregated withdrawals, our approach allows us to preserve part of the catchment-scale heterogeneity while accounting for redundancy induced by nested catchments. The regional analysis showed that the Mediterranean region emerges as a particularly notable hotspot of irrigation

https://doi.org/10.5194/egusphere-2026-4287
Preprint. Discussion started: 17 August 2026

development. Its identification as a major irrigation region is consistent with previous studies (Essa et al., 2023; Tramblay et al., 2020; Sanchis-Ibor et al., 2020; Fader et al., 2016; Hoerling et al., 2012). Because this region combines both high IWW and high positive trends, it appears particularly exposed to future increases in irrigation pressure, it raises important questions regarding future sectoral planning and climate change adaptation. In contrast, the regional analysis identifies Artois–Picardie as an emerging irrigation region. Although current IWW remains comparatively modest, the strong positive trends suggest that irrigation may become increasingly important in the future, extending the development of IWW in that region already documented by Janin (1996). This result suggests that irrigation-related pressures may progressively extend to regions where they have historically played a more limited role.

Although it is a standard approach in trend analysis (Vicente-Serrano et al., 2025; Sa'adi et al., 2019), our approach to quantify trends remains simple. While this provides a robust first-order characterization of long-term changes, it does not characterize potential non-linear dynamics or temporal regime shifts that may occur in IWW. In particular, future work could explore more flexible approaches, such as piecewise regression or non-linear smoothing, or change-point detection methods to better identify potential structural breaks in the time series (Mudelsee, 2019). In addition, we note that trend estimates are conditional on the selected study period and may be sensitive to the choice of the temporal window. Future work could also benefit from exploring longer temporal records, where these are available.

5.3 Relevance for hydrology and climate change impact future studies

The present study complements the framework proposed by Zarpas et al. (2026b). While the latter introduced a data-driven framework to reconstruct annual and monthly IWW over the observation period, the present study extends this framework beyond the observation period by reconstructing temporally consistent annual IWW series. Together, these two studies provide a coherent framework for reconstructing irrigation water withdrawals for hydrological application.

Although temporal disaggregation from annual to monthly scales remains a necessary step, the reconstructed temporally consistent IWW series—and more generally the proposed modelling framework—provide a basis for improving the explicit representation of irrigation in rainfall–runoff models over long time periods and a large sample of catchments. This, in turn, can support more robust assessments of model parameters and improve low flow simulations, where irrigation demand can substantially alter hydrological responses during dry periods (Van Loon et al., 2019).

Beyond hydrological modelling, the proposed framework addresses a major limitation of large-sample irrigation datasets by providing temporally consistent estimates of irrigation withdrawals over a large number of catchments, thereby enabling the extension of regional- to national-scale scenario analyses at the catchment scale (e.g. Sauquet et al., 2026; Arambourou et al., 2025). Moreover, the decomposition into IWW base term and relative deviation term components offers an interpretable separation between structural agricultural conditions and climate-driven variability, making it a promising framework for climate impact assessment and water resources management through scenario exploration.

https://doi.org/10.5194/egusphere-2026-4287
Preprint. Discussion started: 17 August 2026

6 Conclusion

In this paper, we addressed the challenge of performing temporal extrapolation to quantify irrigation water withdrawal (IWW) for a large sample of catchments over a long time period. A temporally stable data-driven approach based on a GAM model was proposed, improving knowledge of IWW trends in France. The key outcomes of this study are:

1. We demonstrated the stability of the GAM modelling framework for data-driven temporal extrapolation of a reference IWW database;
2. We provided insight into IWW in France during the 2000-2007 period, which is a period without actual observations in the national database, by producing annual and catchment-scale time series of IWW for a large sample of catchments in France, while quantifying uncertainties;
3. We documented IWW trends over an extended period in France (2000-2022) while distinguishing the respective contributions of structural factors (via area equipped for irrigation) and climatic variability, highlighting a strong climatic signal and widespread positive trends in IWW.

Overall, we showed that the GAM model is a promising tool for addressing the challenge of temporal extrapolation, due to its additivity, continuity and capacity to handle hierarchical structures. Our study highlighted the trade-off between stability and predictive power, and raises the question of what can be reasonably achieved with a given (not ideal) dataset, as in many real-life applications they can become noisy and uncertain.

Detecting strong and widespread positive trends in IWW across France through a climatic signal is not a surprise, but had never been explicitly documented before. Our robust modelling framework and the result it conveys result raises awareness to important questions for agricultural management, particularly regarding the growing tension between increasing irrigation water demand and increasing pressure on water resources under a changing climate.

By working at the annual timescale, we overlook a decisive trait of irrigation: its seasonality. The disaggregation from annual to monthly IWW estimate should be considered as an important research direction (e.g. by adjusting the fully data-driven methodology developed in Zarpas et al. (2026b)). This step would be essential for irrigation water withdrawal estimation itself, but also for hydrological modeling, and, more broadly, water stress assessment.

Appendix A: Random effect and spatial correlation

Our GAM model can be written in a simplified form as:

$$f^{\mathrm{GAM}}\left(\mathbf{X}_{y,c}\right) = \sum_{i=1,..,n} f_i\left(x_{i,y,c}\right) + Z_c = \boldsymbol{\beta}\mathbf{B}_{y,c} + Z_c, \tag{A1}$$

where $\mathbf{B}_{y,c}$ denotes the vector of spline basis functions evaluated at the predictor values, and $\boldsymbol{\beta}$ the corresponding fitted coefficients. The modeling approach implemented via the mgcv R package actually treats the random effect as penalized

https://doi.org/10.5194/egusphere-2026-4287
Preprint. Discussion started: 17 August 2026

coefficients, and fit the model as a penalized least square. Denoting $\mathbf{Z}$ the random effect vector, the function to be minimized can be written in a simplified form as:

$$L(\boldsymbol{\beta},\mathbf{Z}) = \|\mathcal{W}_{y,c} - (\boldsymbol{\beta}\mathbf{B}_{y,c} + Z_c)\|_{(y,c)} + \lambda \cdot \mathbf{Z}\mathbf{S}\mathbf{Z}^\intercal \tag{A2}$$

where $\|\cdot\|$ is the Euclidian norm, λ is the penalty parameter (found by maximizing the restricted marginal likelihood (REML)), and $\mathbf{S}$ is a penalty matrix. By default, $\mathbf{S}$ is the identity matrix giving:

$$\mathbf{Z}\mathbf{S}\mathbf{Z}^\intercal = \sum_c Z_c^2 \tag{A3}$$

The default penalty thus only shrinks the random effect toward zero and does not account for spatial correlation. Given a known catchment-wise correlation matrix $\mathbf{P} = \left(\rho_{c_i,c_j}\right)$, for example as estimated in Appendix B, we use the Laplacian matrix:

$$\mathbf{S}_{sc} = \mathbf{D} - \mathbf{P} \tag{A4}$$

where $\mathbf{D}$ is the diagonal matrix defined by $D_{ii} = \sum_j P_{i,j}$, referred to as the degree matrix. The customized penalty matrix $\mathbf{S}_{sc}$ yields:

$$\mathbf{Z}\mathbf{S}_{sc}\mathbf{Z}^\intercal = \sum_{i>j} \rho_{c_i,c_j}\left(Z_{c_i} - Z_{c_j}\right)^2 \tag{A5}$$

Hence, our new penalty matrix penalizes differences between catchment's random effect, proportionally to their spatial correlation. We next show in Appendix B how we estimate the catchment-wise spatial correlation.

Appendix B: Catchment-wise spatial correlation estimation

To derive a theoretical expression of the correlation in the spatial random effect, we assume that within each catchment the IWW is randomly distributed with expectation μ and variance V. Let us further assume that it is independently and identically distributed across all catchments. In this framework, the correlation between two disjoint catchments is null and the correlation between nested catchment is given by how much the smallest catchment is nested in the largest one.

More formally, let us consider two catchments C_i and C_j, with $i \neq j$, and let us denote A_i and A_j their respective areas. Without loss of generality, we suppose $C_i \subset C_j$, hence $A_i < A_j$. We further denote W_i and W_j the random IWW on C_i and C_j, respectively. With these assumptions,

$$\mathrm{Cov}(W_i,W_j) = \frac{1}{A_iA_j}\int\limits_{C_i}\int\limits_{C_i} \mathrm{Var}(W_i)d\mathbf{u}d\mathbf{v} + \frac{1}{A_iA_j}\int\limits_{C_i}\int\limits_{C_j\setminus C_i} \mathrm{Cov}(W_i,W_j)d\mathbf{u}d\mathbf{v} = VA_i^2/(A_iA_j) = VA_i/Aj, \tag{B1}$$

with $A_i/A_j < 1$. Since $\mathrm{Var}(W_i) = \mathrm{Var}(W_j) = V$, we thus get that the correlation is $\rho(W_i,W_j) = A_i/A_j < 1$. Finally, one thus gets in all generality

$$\rho(c_i,c_j) = \min(A_i,A_j)/\max(A_i,A_j) \quad \forall i,j. \tag{B2}$$

https://doi.org/10.5194/egusphere-2026-4287
Preprint. Discussion started: 17 August 2026

Appendix C: Regional indicators weighting

The weights $\{w_{c_i}\}_{i=1,n_{\mathcal{R}}}$ used to define the regional indicator for the region $\mathcal{R} = \{c_1, ..., c_{n_{\mathcal{R}}}\}$, containing $n_{\mathcal{R}}$ catchments, are derived from the correlation $\rho(c_i, c_j)$. defined in Eq. (B2). For the catchment c_i, we first compute the quantity $\tilde{w}_{c_i}$:

$$\tilde{w}_{c_i} = \frac{1}{\sum_{j=1,n_{\mathcal{R}}} \rho(c_i, c_j)}. \tag{C1}$$

530 The denominator is the sum of the correlation with all catchments belonging to the same region. The quantity $\tilde{w}_{c_i}$ penalizes catchments that exhibit strong correlation, i.e. strong nesting relationships with other catchments in the same region. Note that since $\rho(c_i, c_i) = 1$ the denominator is always larger than 1 and thus $0 < \tilde{w}_{c_i} \leq 1$. The weight w_{c_i} is then simply defined as the normalized version of $\tilde{w}_{c_i}$:

$$w_{c_i} = \frac{\tilde{w}_{c_i}}{\sum_{j=1,n_{\mathcal{R}}} \tilde{w}_{c_j}} \tag{C2}$$

535 ## Appendix D: Details about uncertainty estimation

D1 Modified log normal law

We assume:

$$\log \hat{\mathcal{W}}_{y,c} \sim \mathcal{N}\left(f^{GAM}(\mathbf{X}_{y,c}), \sigma^2_{y,c}\right), \tag{D1}$$

where $\sigma^2_{y,c}$ is a location-dependent variance term capturing heteroscedastic uncertainty.

540 Under this formulation, the induced distribution of $\mathcal{W}_{y,c}$ is log-normal. Here we use a modified log-normal distribution $\mathcal{LN}^*$ as:

$$\mathcal{LN}^* = \exp\left(-\frac{\sigma^2_{y,c}}{2}\right)\mathcal{LN} \tag{D2}$$

This transformation yields:

$$\mathbb{E}[\hat{\mathcal{W}}_{y,c}] = \exp\left(f^{GAM}(\mathbf{X}_{y,c})\right), \tag{D3}$$

545 This correction has been empirically found to improve predictive performance in cross-validation (not shown) (Lütkepohl and Xu, 2012; Girard et al., 2004).

D2 Estimation of the variance

Our model is given by:

$$\log(\mathcal{W}_{y,c}) = f^{GAM}(\mathbf{X}_{y,c}) + \varepsilon_{y,c} \tag{D4}$$

https://doi.org/10.5194/egusphere-2026-4287
Preprint. Discussion started: 17 August 2026

550 We make the assumption that $\varepsilon_{y,c} \sim N\left(0, \sigma_{err}^2\right)$ and accounts for model bias and irreducible noise. Neglecting the covariance between bias and variance of $f^{GAM}\left(\mathbf{X}_{y,c}\right)$, the predictive uncertainty distribution is:

$$\log \hat{\mathcal{W}}_{y,c} | \mathbf{X}_{y,c} \sim \mathcal{N}\left(f^{GAM}\left(\mathbf{X}_{y,c}\right), \mathrm{var}\left(f^{GAM}\left(\mathbf{X}_{y,c}\right)\right) + \sigma_{err}^2\right) \tag{D5}$$

So, the total log-scale standard deviation is given by:

$$\sigma_{y,c} = \sqrt{\mathrm{var}\left(f^{GAM}\left(\mathbf{X}_{y,c}\right)\right) + \sigma_{err}^2} \tag{D6}$$

555 *Code and data availability.* All data produced and used in this study are publicly available at Zarpas et al. (2026a). All analyses were performed in R (version 4.3.1) using existing, publicly available packages, namely: ggplot2 for figures (Wickham, 2009; Wickham et al., 2007), sf for spatial analysis (Pebesma, 2018, 2016), mgcv for GAM (Wood, 2011, 2000), and modifiedmk for modified Mann Kendall test (Patakamuri and O'Brien, 2017).

Author contributions. **PZ** : Conceptualization, Formal analysis, Investigation, Methodology, Software, Visualization, Writing – original
560 draft, Writing – review & editing ; **MHR** : Conceptualization, Funding acquisition, Supervision, Writing – review & editing; **GT** : Conceptualization, Supervision, Writing – review & editing ; **DA** : Methodology, Writing – review & editing; **FS** : Methodology, Writing – review & editing

Competing interests. One of the authors (FS) is a member of the editorial board of Hydrology and Earth System Sciences.

Acknowledgements. We acknowledge the Etablissement Publique Territoriale de Bassin (EPTB) Eaux & Vilaine, and the project LIFE
565 REVERS'EAU, carried by the region Pays de la Loire and the European Union, for funding the PhD of PZ. We also thank the data producer, Météo-France for SAFRAN product and the OFB for the BNPE. We thank our colleagues from EPTB, Fanny Dubeau, Sebastien Baron and Aldo Penasso, for their stakeholder guidance, and our colleagues from our team Olivier, for his assistance in the publication of the data extraction, and Charles Perrin for his internal review of this paper. We also thanks Benjamin Renard for his advices.

https://doi.org/10.5194/egusphere-2026-4287
Preprint. Discussion started: 17 August 2026

References

Almendra-Martín, L., Martínez-Fernández, J., Piles, M., González-Zamora, , Benito-Verdugo, P., and Gaona, J.: Analysis of soil moisture trends in Europe using rank-based and empirical decomposition approaches, Global and Planetary Change, 215, 103 868, https://doi.org/10.1016/j.gloplacha.2022.103868, 2022.

Amigues, J.-P., Debaeke, P., Itier, B., Lemaire, G., Seguin, B., Tardieu, F., and Thomas, A.: Sécheresse et agriculture. Réduire la vulnérabilité de l'agriculture à un risque accru de manque d'eau, Expertise scientifique collective, synthèse du rappor, INRA, France, 2006.

Arambourou, H. and Ferrière, S.: Quelle évolution de la demande en eau d'ici 2050 ?, Tech. rep., France Stratégie, issue: 148, 2025.

Arambourou, H., Ferrière, S., and Gaillot, A.: L'eau en 2050 : graves tensions sur les écosystèmes et les usages, Tech. rep., Haut-commissariat à la Stratégie et au Plan, Paris, 2025.

Arboleda-Obando, P. F., Ducharne, A., Cheruy, F., and Ghattas, J.: Joint evolution of irrigation, the water cycle and water resources under a strong climate change scenario from 1950 to 2100 in the IPSL-CM6, Earth System Dynamics, 16, 2201–2223, https://doi.org/10.5194/esd-16-2201-2025, 2025.

BNPE: Banque Nationale des Prélèvements Quantitatifs en Eau, https://bnpe.eaufrance.fr/.

Citrini, A., Sangiorgio, M., and Rosa, L.: Global multi-model trends of unsustainable irrigation under climate change scenarios, Environmental Research Letters, 20, 104 011, https://doi.org/10.1088/1748-9326/adfcee, 2025.

Clarotto, L., Allard, D., and Menafoglio, A.: A new class of α -transformations for the spatial analysis of Compositional Data, Spatial Statistics, 47, 100 570, https://doi.org/10.1016/j.spasta.2021.100570, 2022.

Dang, C., Zhang, H., Yao, C., Mu, D., Lyu, F., Zhang, Y., and Zhang, S.: IWRAM: A hybrid model for irrigation water demand forecasting to quantify the impacts of climate change, Agricultural Water Management, 291, 108 643, https://doi.org/10.1016/j.agwat.2023.108643, 2024.

Das, P., Patskoski, J., and Sankarasubramanian, A.: Modeling the Irrigation Withdrawals Over the Coterminous US Using a Hierarchical Modeling Approach, Water Resources Research, 54, 3769–3787, https://doi.org/10.1029/2017WR021723, 2018.

De Wit, A., Boogaard, H., Fumagalli, D., Janssen, S., Knapen, R., Van Kraalingen, D., Supit, I., Van Der Wijngaart, R., and Van Diepen, K.: 25 years of the WOFOST cropping systems model, Agricultural Systems, 168, 154–167, https://doi.org/10.1016/j.agsy.2018.06.018, 2019.

Delaigue, O., Guimarães, G. M., Brigode, P., Génot, B., Perrin, C., Soubeyroux, J.-M., Janet, B., Addor, N., and Andréassian, V.: CAMELS-FR dataset: a large-sample hydroclimatic dataset for France to explore hydrological diversity and support model benchmarking, Earth System Science Data, 17, 1461–1479, https://doi.org/10.5194/essd-17-1461-2025, 2025a.

Delaigue, O., Guimarães, G. M., Génot, B., Lebecherel, L., Brigode, P., and Bourgin, P.-Y.: Database of watershed-scale hydroclimatic observations in France, https://webgr.inrae.fr/eng/tools/databases/bdd-hydroclim, université Paris-Saclay, INRAE, HYCAR Research Unit, Hydrology group, Antony, 2025b.

Döll, P.: Impact of Climate Change and Variability on Irrigation Requirements: A Global Perspective, Climatic Change, 54, 269–293, https://doi.org/10.1023/A:1016124032231, 2002.

Essa, Y. H., Hirschi, M., Thiery, W., El-Kenawy, A. M., and Yang, C.: Drought characteristics in Mediterranean under future climate change, npj Climate and Atmospheric Science, 6, 133, https://doi.org/10.1038/s41612-023-00458-4, 2023.

https://doi.org/10.5194/egusphere-2026-4287
Preprint. Discussion started: 17 August 2026

Fader, M., Shi, S., Von Bloh, W., Bondeau, A., and Cramer, W.: Mediterranean irrigation under climate change: more efficient irrigation needed to compensate for increases in irrigation water requirements, Hydrology and Earth System Sciences, 20, 953–973, https://doi.org/10.5194/hess-20-953-2016, 2016.

Galelli, S., Turner, S. W. D., Pokhrel, Y., Yi Ng., J., Castelletti, A., Bierkens, M. F. P., Pianosi, F., and Biemans, H.: Advancing the Representation of Human Actions in Large-Scale Hydrological Models: Challenges and Future Research Directions, Water Resources Research, 61, e2024WR039 486, https://doi.org/10.1029/2024WR039486, 2025.

García-Garizábal, I., Causapé, J., Abrahao, R., and Merchan, D.: Impact of Climate Change on Mediterranean Irrigation Demand: Historical Dynamics of Climate and Future Projections, Water Resources Management, 28, 1449–1462, https://doi.org/10.1007/s11269-014-0565-7, 2014.

Gaudou, B., Sibertin-Blanc, C., Therond, O., Amblard, F., Auda, Y., Arcangeli, J.-P., Balestrat, M., Charron-Moirez, M.-H., Gondet, E., Hong, Y., and others: The MAELIA multi-agent platform for integrated analysis of interactions between agricultural land-use and low-water management strategies, in: Multi-Agent-Based Simulation XIV: International Workshop, MABS 2013, Saint Paul, MN, USA, May 6-7, 2013, Revised Selected Papers, pp. 85–100, Springer, 2014.

Girard, C., Ouarda, T. B., and Bobée, B.: Étude du biais dans le modèle log-linéaire d'estimation régionale, Canadian Journal of Civil Engineering, 31, 361–368, https://doi.org/10.1139/l03-099, 2004.

Gorguner, M. and Kavvas, M. L.: Modeling impacts of future climate change on reservoir storages and irrigation water demands in a Mediterranean basin, Science of The Total Environment, 748, 141 246, https://doi.org/10.1016/j.scitotenv.2020.141246, 2020.

Haruna, A., Blanchet, J., Evin, G., and Paquet, E.: Regional hotspots and contrasts in the trends of mean and extreme daily precipitation in France, Journal of Hydrology: Regional Studies, 65, 103 378, https://doi.org/10.1016/j.ejrh.2026.103378, 2026.

Hastie, T. and Tibshirani, R.: Generalized Additive Models, Statistical Science, 1, https://doi.org/10.1214/ss/1177013604, 1986.

Hoerling, M., Eischeid, J., Perlwitz, J., Quan, X., Zhang, T., and Pegion, P.: On the Increased Frequency of Mediterranean Drought, Journal of Climate, 25, 2146–2161, https://doi.org/10.1175/JCLI-D-11-00296.1, 2012.

Hsueh, H., Guthke, A., Wöhling, T., and Nowak, W.: Optimized Predictive Coverage by Averaging Time-Windowed Bayesian Distributions, Water Resources Research, 60, e2022WR033 280, https://doi.org/10.1029/2022WR033280, 2024.

Janin, J.-L.: L'irrigation en France depuis 1988, La Houille Blanche, 82, 27–34, https://doi.org/10.1051/lhb/1996083, 1996.

Kragh, S. J., Schneider, R., Fensholt, R., Stisen, S., and Koch, J.: Synthesizing regional irrigation data using machine learning – Towards global upscaling via metamodeling, Agricultural Water Management, 311, 109 404, https://doi.org/10.1016/j.agwat.2025.109404, 2025.

Kreibich, H., Sivapalan, M., AghaKouchak, A., Addor, N., Aksoy, H., Arheimer, B., Arnbjerg-Nielsen, K., Vail-Castro, C., Cudennec, C., Madruga De Brito, M., Di Baldassarre, G., Finger, D. C., Fowler, K., Knoben, W., Krueger, T., Liu, J., Macdonald, E., McMillan, H., Mendiondo, E. M., Montanari, A., Muller, M. F., Pande, S., Tian, F., Viglione, A., Wei, Y., Castellarin, A., Loucks, D. P., Oki, T., Polo, M. J., Savenije, H., Van Loon, A. F., Agarwal, A., Alvarez-Garreton, C., Andreu, A., Barendrecht, M. H., Brunner, M., Cavalcante, L., Cavus, Y., Ceola, S., Chaffe, P., Chen, X., Coxon, G., Dandan, Z., Davary, K., Dembélé, M., Dewals, B., Frolova (Bibikova), T., Gain, A. K., Gelfan, A., Ghoreishi, M., Grabs, T., Guan, X., Hannah, D. M., Helmschrot, J., Höllermann, B., Hounkpè, J., Koebele, E., Konar, M., Kratzert, F., Lindersson, S., Llasat, M. C., Matanó, A., Mazzoleni, M., Mejia, A., Mendoza, P., Merz, B., Mukherjee, J., Nasiri Saleh, F., Nlend, B., Nonki, R. M., Orieschnig, C., Papagiannaki, K., Penny, G., Petrucci, O., Pimentel, R., Pool, S., Ridolfi, E., Rusca, M., Sairam, N., Sankaran Namboothiri, A., Sarmento Buarque, A. C., Savelli, E., Schoppa, L., Schröter, K., Scolobig, A., Shafiei, M., Sikorska-Senoner, A. E., Smigaj, M., Teutschbein, C., Thaler, T., Todorovic, A., Tootoonchi, F., Tootoonchi, R., Toth, E., Van Nooijen, R., Vanelli, F. M., Vásquez, N., Walker, D. W., Wens, M., Yu, D. J., Zarei, H., Zhou, C., and Blöschl, G.: Panta Rhei: a decade of progress in research

https://doi.org/10.5194/egusphere-2026-4287
Preprint. Discussion started: 17 August 2026

on change in hydrology and society, Hydrological Sciences Journal, 70, 1210–1236, https://doi.org/10.1080/02626667.2025.2469762, 2025.

Lamb, S. E., Haacker, E. M. K., and Smidt, S. J.: Influence of Irrigation Drivers Using Boosted Regression Trees: Kansas High Plains, Water Resources Research, 57, e2020WR028 867, https://doi.org/10.1029/2020WR028867, 2021.

Linga, S. N., Aguiló-Rivera, C., Larsen, J., Massimi, M., Wei, N., and Puy, A.: Global Irrigation Modeling Relies More on Pragmatic Than Empirical Assumptions, Water Resources Research, 61, e2025WR040 674, https://doi.org/10.1029/2025WR040674, 2025.

Linés, C. and Werner, M.: How useful are seasonal forecasts for farmers facing drought? A user-based modelling approach, Climate Services, 39, 100 595, https://doi.org/10.1016/j.cliser.2025.100595, 2025.

Lütkepohl, H. and Xu, F.: The role of the log transformation in forecasting economic variables, Empirical Economics, 42, 619–638, https://doi.org/10.1007/s00181-010-0440-1, 2012.

Marra, G. and Wood, S. N.: Practical variable selection for generalized additive models, Computational Statistics & Data Analysis, 55, 2372–2387, https://doi.org/10.1016/j.csda.2011.02.004, 2011.

Marra, G. and Wood, S. N.: Coverage Properties of Confidence Intervals for Generalized Additive Model Components, Scandinavian Journal of Statistics, 39, 53–74, https://doi.org/10.1111/j.1467-9469.2011.00760.x, 2012.

Mehta, P., Siebert, S., Kummu, M., Deng, Q., Ali, T., Marston, L., Xie, W., and Davis, K. F.: Half of twenty-first century global irrigation expansion has been in water-stressed regions, Nature Water, 2, 254–261, https://doi.org/10.1038/s44221-024-00206-9, 2024.

Muckley, E. S., Saal, J. E., Meredig, B., Roper, C. S., and Martin, J. H.: Interpretable models for extrapolation in scientific machine learning, Digital Discovery, 2, 1425–1435, https://doi.org/10.1039/D3DD00082F, 2023.

Mudelsee, M.: Trend analysis of climate time series: A review of methods, Earth-Science Reviews, 190, 310–322, https://doi.org/10.1016/j.earscirev.2018.12.005, 2019.

Nicolle, P., Andréassian, V., Royer-Gaspard, P., Perrin, C., Thirel, G., Coron, L., and Santos, L.: Technical note: RAT – a robustness assessment test for calibrated and uncalibrated hydrological models, Hydrology and Earth System Sciences, 25, 5013–5027, https://doi.org/10.5194/hess-25-5013-2021, 2021.

Nie, W., Zaitchik, B. F., Rodell, M., Kumar, S. V., Arsenault, K. R., and Badr, H. S.: Irrigation Water Demand Sensitivity to Climate Variability Across the Contiguous United States, Water Resources Research, 57, 2020WR027 738, https://doi.org/10.1029/2020WR027738, 2021.

Patakamuri, S. K. and O'Brien, N.: modifiedmk: Modified Versions of Mann Kendall and Spearman's Rho Trend Tests, https://doi.org/10.32614/CRAN.package.modifiedmk, institution: Comprehensive R Archive Network Pages: 1.6, 2017.

Pebesma, E.: sf: Simple Features for R, https://doi.org/10.32614/CRAN.package.sf, institution: Comprehensive R Archive Network Pages: 1.1-1, 2016.

Pebesma, E.: Simple Features for R: Standardized Support for Spatial Vector Data, https://doi.org/10.32614/RJ-2018-009, 2018.

Pedersen, E. J., Miller, D. L., Simpson, G. L., and Ross, N.: Hierarchical generalized additive models in ecology: an introduction with mgcv, PeerJ, 7, e6876, https://doi.org/10.7717/peerj.6876, 2019.

Portoghese, I., Matarrese, R., Mirra, L., and Giannoccaro, G.: Assimilating Farmers' Behaviour in the Development of an ET-Based Irrigation Water-Accounting Model, Water Resources Management, 39, 7749–7774, https://doi.org/10.1007/s11269-025-04316-1, 2025.

Puy, A., Borgonovo, E., Lo Piano, S., Levin, S. A., and Saltelli, A.: Irrigated areas drive irrigation water withdrawals, Nature Communications, 12, 4525, https://doi.org/10.1038/s41467-021-24508-8, 2021.

Puy, A., Beneventano, P., Levin, S. A., Lo Piano, S., Portaluri, T., and Saltelli, A.: Models with higher effective dimensions tend to produce more uncertain estimates, Science Advances, 8, eabn9450, https://doi.org/10.1126/sciadv.abn9450, 2022a.

https://doi.org/10.5194/egusphere-2026-4287
Preprint. Discussion started: 17 August 2026

Puy, A., Sheikholeslami, R., Gupta, H. V., Hall, J. W., Lankford, B., Lo Piano, S., Meier, J., Pappenberger, F., Porporato, A., Vico, G., and Saltelli, A.: The delusive accuracy of global irrigation water withdrawal estimates, Nature Communications, 13, 3183, https://doi.org/10.1038/s41467-022-30731-8, 2022b.

Puy, A., Linga, S. N., Wei, N., Flinders, S., Callow, B., Allen, G., Cross, B., Aguiló-Rivera, C., and Lankford, B.: Widely cited global irrigation statistics lack empirical support, PNAS Nexus, 4, pgaf323, https://doi.org/10.1093/pnasnexus/pgaf323, 2025.

Ribes, A., Boé, J., Qasmi, S., Dubuisson, B., Douville, H., and Terray, L.: An updated assessment of past and future warming over France based on a regional observational constraint, Earth System Dynamics, 13, 1397–1415, https://doi.org/10.5194/esd-13-1397-2022, 2022.

Roberts, D. R., Bahn, V., Ciuti, S., Boyce, M. S., Elith, J., Guillera-Arroita, G., Hauenstein, S., Lahoz-Monfort, J. J., Schröder, B., Thuiller, W., Warton, D. I., Wintle, B. A., Hartig, F., and Dormann, C. F.: Cross-validation strategies for data with temporal, spatial, hierarchical, or phylogenetic structure, Ecography, 40, 913–929, https://doi.org/10.1111/ecog.02881, 2017.

Sanchis-Ibor, C., Molle, F., and Kuper, M.: Irrigation and water governance, in: Water Resources in the Mediterranean Region, pp. 77–106, Elsevier, https://doi.org/10.1016/B978-0-12-818086-0.00004-2, 2020.

Sangha, L. and Shortridge, J.: Quantification of unreported water use for supplemental crop irrigation in humid climates using publicly available agricultural data, Agricultural Water Management, 287, 108 402, https://doi.org/10.1016/j.agwat.2023.108402, 2023.

Santos, L., Thomas, A., Tallec, G., Mounereau, L., Bluche, A., Lemaire, B. J., Louafi, R., and Thirel, G.: Exploring future water resources and uses considering water demand scenarios and climate change for the French Sèvre Nantaise basin, Hydrology and Earth System Sciences, 30, 1915–1949, https://doi.org/10.5194/hess-30-1915-2026, 2026.

Sauquet, E., Evin, G., Siauve, S., Aissat, R., Arnaud, P., Bérel, M., Bonneau, J., Branger, F., Caballero, Y., Colléoni, F., Ducharne, A., Gailhard, J., Habets, F., Hendrickx, F., Héraut, L., Hingray, B., Huang, P., Jaouen, T., Jeantet, A., Lanini, S., Le Lay, M., Magand, C., Mimeau, L., Monteil, C., Munier, S., Perrin, C., Robelin, O., Rousset, F., Soubeyroux, J.-M., Strohmenger, L., Thirel, G., Tocquer, F., Tramblay, Y., Vergnes, J.-P., and Vidal, J.-P.: A large transient multi-scenario multi-model ensemble of future streamflow and groundwater projections in France, Hydrology and Earth System Sciences, 30, 2277–2300, https://doi.org/10.5194/hess-30-2277-2026, 2026.

Sa'adi, Z., Shahid, S., Ismail, T., Chung, E.-S., and Wang, X.-J.: Trends analysis of rainfall and rainfall extremes in Sarawak, Malaysia using modified Mann–Kendall test, Meteorology and Atmospheric Physics, 131, 263–277, https://doi.org/10.1007/s00703-017-0564-3, 2019.

Sen, P. K.: Estimates of the Regression Coefficient Based on Kendall's Tau, Journal of the American Statistical Association, 63, 1379–1389, https://doi.org/10.1080/01621459.1968.10480934, 1968.

Shortridge, J.: Prediction of multi-sectoral longitudinal water withdrawals using hierarchical machine learning models, Journal of Hydroinformatics, 25, 2389–2405, https://doi.org/10.2166/hydro.2023.110, 2023.

Soutif-Bellenger, M., Thirel, G., Therond, O., and Villerd, J.: As simple as possible but not simpler?: the case of irrigation modeling at catchment scale in southwestern France, Irrigation Science, 41, 713–736, https://doi.org/10.1007/s00271-023-00846-x, 2023.

Sédillot, B., Cahen, H., Courtier, L., Antea, and Agence Citizen Press: L'irrigation des surfaces agricoles : évolution entre 2010 et 2020, Tech. rep., https://www.statistiques.developpement-durable.gouv.fr/lirrigation-des-surfaces-agricoles-evolution-entre-2010-et-2020, 2024.

Thirel, G., Andréassian, V., and Perrin, C.: On the need to test hydrological models under changing conditions, Hydrological Sciences Journal, 60, 1165–1173, https://doi.org/10.1080/02626667.2015.1050027, 2015.

Tian, X., Dong, J., Jin, S., He, H., Yin, H., and Chen, X.: Climate change impacts on regional agricultural irrigation water use in semi-arid environments, Agricultural Water Management, 281, 108 239, https://doi.org/10.1016/j.agwat.2023.108239, 2023.

Tramblay, Y., Llasat, M. C., Randin, C., and Coppola, E.: Climate change impacts on water resources in the Mediterranean, Regional Environmental Change, 20, 83, s10 113–020–01 665–y, https://doi.org/10.1007/s10113-020-01665-y, 2020.

Tsipras, D., Santurkar, S., Engstrom, L., Turner, A., and Madry, A.: Robustness May Be at Odds with Accuracy, in: International Conference on Learning Representations, https://openreview.net/forum?id=SyxAb30cY7, 2019.

Twardosz, R., Walanus, A., and Guzik, I.: Warming in Europe: Recent Trends in Annual and Seasonal temperatures, Pure and Applied Geophysics, 178, 4021–4032, https://doi.org/10.1007/s00024-021-02860-6, 2021.

Van De Pol, M. and Wright, J.: A simple method for distinguishing within- versus between-subject effects using mixed models, Animal Behaviour, 77, 753–758, https://doi.org/10.1016/j.anbehav.2008.11.006, 2009.

Van Loon, A. F., Rangecroft, S., Coxon, G., Breña Naranjo, J. A., Van Ogtrop, F., and Van Lanen, H. A. J.: Using paired catchments to quantify the human influence on hydrological droughts, Hydrology and Earth System Sciences, 23, 1725–1739, https://doi.org/10.5194/hess-23-1725-2019, 2019.

Vicente-Serrano, S. M., Tramblay, Y., Reig, F., González-Hidalgo, J. C., Beguería, S., Brunetti, M., Kalin, K. C., Patalen, L., Kržič, A., Lionello, P., Lima, M. M., Trigo, R. M., El-Kenawy, A. M., Eddenjal, A., Türkes, M., Koutroulis, A., Manara, V., Maugeri, M., Badi, W., Mathbout, S., Bertalanič, R., Bocheva, L., Dabanli, I., Dumitrescu, A., Dubuisson, B., Sahabi-Abed, S., Abdulla, F., Fayad, A., Hodzic, S., Ivanov, M., Radevski, I., Peña-Angulo, D., Lorenzo-Lacruz, J., Domínguez-Castro, F., Gimeno-Sotelo, L., García-Herrera, R., Franquesa, M., Halifa-Marín, A., Adell-Michavila, M., Noguera, I., Barriopedro, D., Garrido-Perez, J. M., Azorin-Molina, C., Andres-Martin, M., Gimeno, L., Nieto, R., Llasat, M. C., Markonis, Y., Selmi, R., Ben Rached, S., Radovanović, S., Soubeyroux, J.-M., Ribes, A., Saidi, M. E., Bataineh, S., El Khalki, E. M., Robaa, S., Boucetta, A., Alsafadi, K., Mamassis, N., Mohammed, S., Fernández-Duque, B., Cheval, S., Moutia, S., Stevkov, A., Stevkova, S., Luna, M. Y., and Potopová, V.: High temporal variability not trend dominates Mediterranean precipitation, Nature, 639, 658–666, https://doi.org/10.1038/s41586-024-08576-6, 2025.

Von Korff, M. and Sander, T.: Limits of Prediction for Machine Learning in Drug Discovery, Frontiers in Pharmacology, 13, 832 120, https://doi.org/10.3389/fphar.2022.832120, 2022.

Vu, H., Shanafield, M., Nhat, T., Partington, D., and Batelaan, O.: Mapping catchment-scale unmonitored groundwater abstractions: Approaches based on soft data, Journal of Hydrology: Regional Studies, 30, 100 695, https://doi.org/10.1016/j.ejrh.2020.100695, 2020.

Warziniack, T., Arabi, M., Brown, T. C., Froemke, P., Ghosh, R., Rasmussen, S., and Swartzentruber, R.: Projections of Freshwater Use in the United States Under Climate Change, Earth's Future, 10, e2021EF002 222, https://doi.org/10.1029/2021EF002222, 2022.

Wickham, H.: ggplot2: Elegant Graphics for Data Analysis, Springer New York, New York, NY, https://doi.org/10.1007/978-0-387-98141-3, 2009.

Wickham, H., Chang, W., Henry, L., Pedersen, T. L., Takahashi, K., Wilke, C., Woo, K., Yutani, H., Dunnington, D., and Van Den Brand, T.: ggplot2: Create Elegant Data Visualisations Using the Grammar of Graphics, https://doi.org/10.32614/CRAN.package.ggplot2, institution: Comprehensive R Archive Network Pages: 4.0.3, 2007.

Wikle, C. K., Zammit Mangion, A., and Cressie, N. A. C.: Spatio-temporal statistics with R, Chapman & Hall/CRC the R series, CRC Press, Boca Raton London New York, 2019.

Wood, S.: mgcv: Mixed GAM Computation Vehicle with Automatic Smoothness Estimation, https://doi.org/10.32614/CRAN.package.mgcv, institution: Comprehensive R Archive Network Pages: 1.9-4, 2000.

Wood, S. N.: Fast stable restricted maximum likelihood and marginal likelihood estimation of semiparametric generalized linear models, issue: 1 Pages: 3–36 Publication Title: Journal of the Royal Statistical Society (B) Volume: 73, 2011.

Yu, Y., Zhang, G., Qi, P., Sun, J., Zhang, Q., Hu, B., and Xu, Y.: Irrigated agriculture expansion drives groundwater storage decline in Black Soil Region of Northeast China, Agricultural Water Management, 319, 109 813, https://doi.org/10.1016/j.agwat.2025.109813, 2025.

https://doi.org/10.5194/egusphere-2026-4287
Preprint. Discussion started: 17 August 2026

Yue, S. and Wang, C.: The Mann-Kendall Test Modified by Effective Sample Size to Detect Trend in Serially Correlated Hydrological Series, Water Resources Management, 18, 201–218, https://doi.org/10.1023/B:WARM.0000043140.61082.60, 2004.

Zarpas, P., Ramos, M.-H., and Tallec, G.: Assessing trends in irrigation water withdrawal using a data-driven temporal extrapolation framework, https://doi.org/10.57745/GZHS9F, 2026a.

Zarpas, P., Ramos, M.-H., Tallec, G., Allard, D., and Sarrazin, F. J.: A data-driven framework to estimate irrigation water withdrawal for hydrological modeling, https://doi.org/10.22541/essoar.177100458.87254479/v1, 2026b.

Zhang, H., Yu, Y., Jiao, J., Xing, E., Ghaoui, L. E., and Jordan, M.: Theoretically Principled Trade-off between Robustness and Accuracy, in: Proceedings of the 36th International Conference on Machine Learning, edited by Chaudhuri, K. and Salakhutdinov, R., vol. 97 of *Proceedings of Machine Learning Research*, pp. 7472–7482, PMLR, https://proceedings.mlr.press/v97/zhang19p.html, 2019.

Zhang, L., Zheng, D., Zhang, K., Chen, H., Ge, Y., and Li, X.: Divergent trends in irrigation-water withdrawal and consumption over mainland China, Environmental Research Letters, 17, 094 001, https://doi.org/10.1088/1748-9326/ac8606, 2022.

Zhang, L., Ma, H., Hu, Y., Wang, Y., Ma, Q., and Zhao, Y.: On the Use of Knowledge-Informed Machine Learning and Multisource Data for Spatially Explicit Estimation of Irrigation Water Withdrawal, Earth's Future, 13, e2025EF006 704, https://doi.org/10.1029/2025EF006704, 2025.

Zhu, W. and Siebert, S.: Climate-driven interannual variability in subnational irrigation areas across Europe, Communications Earth & Environment, 5, 554, https://doi.org/10.1038/s43247-024-01721-z, 2024.

Řehoř, J., Trnka, M., Brázdil, R., Fischer, M., Balek, J., Van Der Schrier, G., and Feng, S.: Global hotspots in soil moisture-based drought trends, Environmental Research Letters, 19, 014 021, https://doi.org/10.1088/1748-9326/ad0f01, 2024.